A depth-averaged two-phase model for fluvial sediment-laden flows over erodible beds

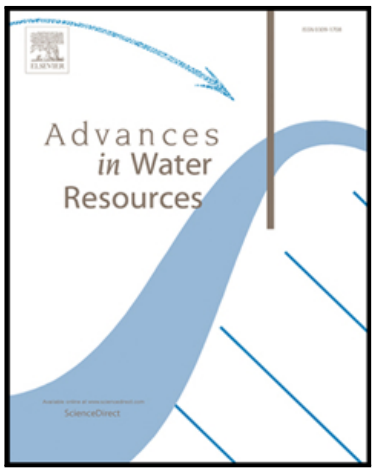

A depth-averaged two-phase model for fluvial sediment-laden flows over erodible beds

Ji Li , Zhixian Cao , Honglu Qian , Qingquan Liu , Gareth Pender

PII: S0309-1708(17)30149-5
DOI: 10.1016/j.advwatres.2017.08.014
Reference: ADWR 2927

To appear in: *Advances in Water Resources*

Received date: 15 February 2017
Revised date: 20 August 2017
Accepted date: 22 August 2017

Please cite this article as: Ji Li , Zhixian Cao , Honglu Qian , Qingquan Liu , Gareth Pender , A depth-averaged two-phase model for fluvial sediment-laden flows over erodible beds, *Advances in Water Resources* (2017), doi: 10.1016/j.advwatres.2017.08.014

Highlights:

- A depth-averaged two-phase model is proposed for fluvial sediment-laden flows.
- The model well reproduces a series of typical cases.
- It resolves that finer sediment is transported faster than coarser grains.

A depth-averaged two-phase model for fluvial sediment-laden flows over erodible beds

Ji Li [a], Zhixian Cao [a, *], Honglu Qian [a], Qingquan Liu [b], Gareth Pender [c]

[a] *State Key Laboratory of Water Resources and Hydropower Engineering Science, Wuhan University, Wuhan, 430072, China*

[b] *Department of Mechanics, Beijing Institute of Technology, Beijing, 100081, China*

[c] *Institute for Infrastructure and Environment, Heriot-Watt University, Edinburgh Campus, Edinburgh, EH14 4AS, UK*

* Corresponding author: Zhixian Cao

Email addresses: lijimy0321@whu.edu.cn (J. Li), zxcao@whu.edu.cn (Z. Cao), qianhonglu@whu.edu.cn (H. Qian), liuqq@bit.edu.cn (Q. Liu), g.pender@hw.ac.uk (G. Pender)

Abstract

Fluvial sediment-laden flow represents a class of fluid-solid two-phase flows, which typically involve multi grain sizes, interphase and particle-particle interactions, and mass exchange with the bed. However, existing depth-averaged models ignore one or more of these physical aspects. Here a physically enhanced, coupled depth-averaged two-phase model is proposed for fluvial sediment-laden flow, which explicitly incorporates all these aspects and also turbulent Reynolds stresses. A well-balanced numerical algorithm is applied to solve the governing equations of the model. The present model is benchmarked against a series of typical cases, concerning refilling of a dredged trench, bed aggradation due to sediment overloading, and flood flows due to landslide dam failure. It features encouraging performance as compared to measured data and a quasi single-phase mixture model. The present model reveals that the larger the grain size, the slower the sediment fraction transports, which concurs with prior findings from experimental observations and field data. Also, the fluid phase Reynolds stresses are considerable where the flow rapidly varies, whilst the solid phase Reynolds stresses are negligible if sediment concentration is sufficiently low.

Keywords: *open channel flow; sediment-laden flow; shallow water; two-phase model; erodible bed; multi grain sizes*

1. Introduction

Fluvial flows can induce sediment transport and morphological changes, which in turn conspire to modify the flows (Cao et al. 2017). Accordingly, there exist active interactions among the flow, sediment and morphology, and also among particles with different grain sizes. Physically, fluvial sediment-laden flow over erodible beds is a typical class of fluid-solid two-phase flows, involving multi grain sizes, interphase and particle-particle interactions, and mass exchange between the flow and the bed. Refined modelling of fluvial sediment-laden flows over erodible beds is essential for not only river engineering practice, but also flood risk management and environmental protection (Wu 2007; Frey and Church 2009).

In principle, mathematical models for fluvial sediment-laden flows can be divided into two distinct categories, i.e., depth-resolving models and depth-averaged models. While the depth-resolving models can resolve detailed evolution process and vertical structure of fluvial sediment-laden flows from either single-phase flow perspective (e.g., Wu et al. 2000; Fang and Wang 2000; Marsooli and Wu 2015) or two-phase flow viewpoint (e.g., Drew 1983; Greimann et al. 1999; Greimann and Holly 2001; Hsu et al. 2003; Longo 2005; Chauchat and Guillou 2008; Chiodi et al. 2014), they require excessively high computing costs and thus may not be unrealistic for large-scale prototype river engineering applications. Comparatively, depth-averaged models have been widely used in modelling fluvial sediment-laden flows over erodible beds. This is sensible because a balance between theoretical integrity and practical applicability can be achieved.

Most depth-averaged models for fluvial sediment-laden flows to date are based on the quasi single-phase perspective, which regards the fluid (water) and solid (sediment) mixture as a single-phase fluid (e.g., Armanini and Di Silvio 1988; Cui et al. 1996; Hoey and Ferguson 1994; Cao et al. 2004; Wu 2004, 2007; Wu and Wang 2008; Viparelli et al. 2010; Hu et al. 2014; Qian et al. 2015; Guan et al. 2016). In general, these depth-averaged models cannot resolve the vertical profiles of velocity and sediment concentration. In this regard, it is noted that in some “enhanced” depth-averaged quasi single-phase mixture models, especially those for the sediment-laden flows in meandering or curved channels, presumed vertical profiles of velocity and sediment concentration are incorporated in

the depth-averaging procedure and thus modified results could be obtained (e.g., Yeh and Kennedy 1993; Guo and Jin 1999; Wu 2007; Vasquez et al. 2011; Uchida and Fukuoka 2014). Yet, the modelling accuracy of such models largely depends on the presumed vertical profile function (Xia and Jin 2008). Generally, depth-averaged quasi single-phase mixture model only incorporate a single momentum conservation equation for the water-sediment mixture, despite the fact that the respective mass conservation equations for the water-sediment mixture and sediment phases. Consequently, only the depth-averaged velocity of water-sediment mixture is solved numerically, while the depth-averaged velocities of the sediment phases are *a priori* empirically determined by the mixture velocity along with the modification coefficient β (normally $\beta \leq 1$), which is originally developed for a single size class of sediments due to the experimental data. Albeit far from perfect from theoretical perspectives, the depth-averaged quasi single-phase mixture models to date actually perform well and achieve satisfactory results in modelling fluvial sediment-laden flows over erodible beds. More broadly, they have been extended to sharply stratified processes, for which the double layer-averaged quasi single-phase mixture models are warranted (Li et al. 2013; Cao et al. 2015b; Zech et al. 2015). However, interphase (water-to-sediment) and particle-particle interactions, which characterize the fluid-solid two-phase flows, need to be incorporated and estimated properly in modelling fluvial sediment-laden flows. Briefly, for fluvial processes, bed-load velocity is appreciably lower than the flow (Chien and Wan 1999; Wu et al. 2006; Greimann et al. 2008), and a velocity lag between the flow and the suspended load sediments is also observed in experiments (Muste et al. 2005), both of which actually feature interphase interactions. Moreover, sediment particles of different grain sizes feature different velocities (Drake et al. 1988; Wilcock 1997; Ferguson and Wathen 1998; Lenzi 2004), characterizing particle-particle interactions. In this regard, two-phase modelling shows great promise for fluvial sediment-laden flows modelling as more refined physical mechanisms are accommodated. Specifically, the fluid and solid phases are resolved separately due to their respective mass and momentum conservation laws.

While depth-averaged two-phase models have been used extensively in the field of earth surface flows such as debris flows and granular flows (e.g., Pitman and Le 2005; Pudasaini 2012; Bouchut et

al. 2015), their applications and developments for fluvial processes remain at the early stage, arguably due to the complexity of numerical solution and the demand for extra relationships to close the governing equations. Notably, based on the work of Greco et al. (2012), an extended depth-averaged two-phase model is proposed for modeling dam-break flows over erodible beds (Di Cristo et al. 2016). Yet, their models are confined to single-sized sediment transport (i.e., the sediment size is kept at a single value, normally the median or mean sediment diameter, throughout the modeling). Indeed, existing depth-averaged two-phase modes for not only fluvial processes, but also earth surface flows, have exclusively not incorporated multi grain sizes of sediments. Clearly, the models assuming a single size of sediments cannot reflect the nature of fluvial sediment-laden flows, typically characterized by broad particle size-distribution. For example, downstream fining is rather common in natural rivers (Paola et al. 1992). As a consequence, there is a lack of physically enhanced models available for resolving the depth-averaged size-specific longitudinal sediment velocity, which is however critical to dynamics of sediment transport (Haschenburger and Church 1998; Greimann 2003). Notably, the finding that the depth-averaged longitudinal sediment velocity decreases with increasing grain size in non-uniform sediment transport has not yet been reproduced numerically by existing depth-averaged models, although it has been revealed for long from experiment observations (Wilcock 1997) and field data (Drake et al. 1988; Ferguson and Wathen 1998; Lenzi 2004).

Here a coupled depth-averaged two-phase model is presented for fluvial sediment-laden flows over erodible beds, accommodating multi grain sizes, interphase and particle-particle interactions, mass exchange between the flow and the bed as well as the depth-averaged turbulent Reynolds stresses. Essentially, multi grain sizes of sediments are explicitly incorporated in the present model, representing a step forward as compared to existing depth-averaged two-phase model based on single-sized sediment transport. Also, the present model is capable of resolving the interphase and particle-particle interactions numerically rather than by the empirical relationship, which is used in depth-averaged quasi single-phase mixture models. A well-balanced algorithm, employing the surface gradient method along with the finite volume SLIC scheme, is used to solve the governing equations. The present depth-averaged two-phase model is tested against a series of cases, concerning refilling of

a dredged trench (van Rijn 1986; Armanini and Di Silvio 1988), bed aggradation due to sediment overloading (Seal et al. 1997), and flood flows due to landslide dam failure (Cao et al. 2011). The model has also been compared with existing depth-averaged quasi single-phase models (Qian et al. 2015).

2. Mathematical model

2.1. Governing equations

Consider one-dimensional fluvial sediment-laden flows over erodible beds composed of non-cohesive sediments with N size classes. Let d_k denotes the diameter of k th size of the sediments, where subscript $k = 1, 2, ..., N$. Sediment feeding is included, while the fed materials are assumed to enter the water-sediment mixture directly. The model is based on the three-layer structure, incorporating the bed load layer, the active layer and the substrate layer (Hirano, 1971; Parker, 1991a, b). Following Qian et al. (2015), the bed load layer is extended to the sediment transport layer, in which both the bed load and the suspended load may coexist. The active layer is located between the sediment transport layer and the substrate layer. Sediments within the active layer are assumed to be well mixed in the vertical and can exchange freely with the upper and lower layers. The substrate layer with certain structure is known as the stratigraphy of the deposit and may vary temporally.

On the basis of continuum theory for both the fluid phase (water) and the solid phase (sediment), a set of one-dimensional depth-averaged equations for the mass and momentum conservation for the fluid-solid mixture, fluid and solid phases is developed by transforming the basic three-dimensional two-phase flow equations (Pai 1977) into a relatively simple set of equations. Here sediment concentration (solid fraction) is presumed not to be too low to negate the applicability of the continuum assumption, though a threshold value is not yet available to date. Moreover, "depth-averaged" illustrates that the physical quantities (velocity and volume fraction) are integrated and averaged along the depth of the flow. In the present study, the shape factor, which arises from the depth-averaging procedure and represents the effects of non-uniformity of vertical structure of velocity

and sediment concentration, are presumed to be unit. Indeed, it is a conventional practice in shallow water hydro-sediment-morphodynamics models (Wu et al. 2007), which implies the effects of shape factors are neglected. However, this practice does not mean that the velocity and sediment concentration are assumed to be constant along the flow depth. The depth-averaged turbulent Reynolds stresses for both the fluid and solid phases can be readily obtained through the conventional Reynolds averaging procedure. In general, there exist interactions among flow, sediments and erodible bed and also among particles of different grain sizes. Coupled modelling is generally justified, which has been more and more implemented in computational rive dynamics since the work of Cao et al. 2004. This is followed in the present depth-averaged two-phase model. The detailed derivation of the depth-averaged governing equations is given in Supplementary A.

The depth-averaged mass and momentum conservation equations for the fluid-solid mixture are

$$\frac{\partial}{\partial t}\rho_m h+\frac{\partial}{\partial x}\rho_m hU_m=-\rho_0\frac{\partial z_b}{\partial t}+\rho_s\frac{\Gamma}{B} \tag{1}$$

$$\begin{aligned}\frac{\partial \rho_m hU_m}{\partial t}+\frac{\partial}{\partial x}(\rho_m hU_m^2+\frac{1}{2}\rho_m gh^2)=&-\tau_b-\rho_m gh\frac{\partial z_b}{\partial x}+\frac{\partial}{\partial x}[hT_R+hT_\mu]\\&-\frac{\partial}{\partial x}h\sum[\rho_s C_k i_{s_k}(i_{s_k}-i_f)]\end{aligned} \tag{2}$$

The depth-averaged mass and momentum conservation equations for the solid phase are

$$\frac{\partial \rho_s h_{sk}}{\partial t}+\frac{\partial \rho_s h_{sk}U_{sk}}{\partial x}=\rho_s F_k+\rho_s\frac{\Gamma_k}{B} \tag{3}$$

$$\begin{aligned}\frac{\partial \rho_s h_{sk}U_{sk}}{\partial t}+\frac{\partial}{\partial x}(\rho_s h_{sk}U_{sk}^2+\frac{1}{2}C_k\rho_m gh^2)=&-\tau_{s_k b}-\rho_m gh_{sk}\frac{\partial z_b}{\partial x}+\frac{\partial}{\partial x}[h_{sk}T_{Rs_k}+h_{sk}T_{\mu s_k}]\\&+F_{s_k f}+F_{s-s_k}+\frac{1}{2}\rho_m gh^2\frac{\partial C_k}{\partial x}\end{aligned} \tag{4}$$

The depth-averaged mass and momentum conservation equations for the fluid phase are

$$\frac{\partial \rho_f h_f}{\partial t}+\frac{\partial \rho_f h_f U_f}{\partial x}=\rho_f p\frac{F_T}{1-p} \tag{5}$$

$$\frac{\partial \rho_f h_f U_f}{\partial t}+\frac{\partial}{\partial x}(\rho_f h_f U_f^2+\frac{1}{2}C_f\rho_m g h^2)=-\tau_{fb}-\rho_m g h_f\frac{\partial z_b}{\partial x}+\frac{\partial}{\partial x}[h_f T_{Rf}+h_f T_{\mu f}] -\sum(F_{s_k f})+\frac{1}{2}\rho_m g h^2\frac{\partial C_f}{\partial x} \tag{6}$$

The bed deformation equation is

$$\frac{\partial z_b}{\partial t}=-\frac{F_T}{1-p} \tag{7}$$

The active layer equation is

$$\frac{\partial h_a f_{ak}}{\partial t}+f_{Ik}\frac{\partial \xi}{\partial t}=-\frac{F_k}{1-p} \tag{8}$$

where t is the time, x is the streamwise coordinate; g is the gravitational acceleration; the subscripts f, s and m denote the fluid, solid and fluid-solid mixture respectively; h is the depth of the fluid-solid mixture, z_b is the bed elevation; $h_{sk}=C_k h$ is the size-specific thickness of the solid phase and C_k is the depth-averaged size-specific volumetric sediment concentration; $C_T=\sum C_k$ is the depth-averaged total sediment concentration; $h_f=C_f h$ is the thickness of the fluid phase and $C_f=1-C_T$ is the depth-averaged volume fraction of the fluid phase; Γ_k and Γ are the size-specific and total sediment feeding rates per unit channel length, $\Gamma=\sum\Gamma_k$; B is the channel width; ρ_f, ρ_s are the densities of the water and sediment respectively, $\rho_m=\rho_s C_T+\rho_f(1-C_T)$ is the density of the fluid-solid mixture; $\rho_0=\rho_f p+\rho_s(1-p)$ is the density of the bed materials, p is the bed sediment porosity; U_{sk} is the depth-averaged size-specific velocity of the solid phase in the $x-$ direction, U_f is the depth-averaged velocity of the fluid phase in the $x-$ direction; U_m is the depth-averaged velocity of the water-sediment mixture in the $x-$ direction, and U_m is defined as $\rho_m U_m=\sum(\rho_s U_{sk}C_k)+\rho_f U_f C_f$ according to mass flux conservation; $i_{s_k}=U_{sk}-U_m$, $i_f=U_f-U_m$ denote the differences among the size-specific sediment phase velocity U_{sk}, the fluid phase velocity U_f and the fluid-solid mixture velocity U_m; τ_b, $\tau_{s_k b}$, τ_{fb} are the bed shear stresses for the fluid-solid

mixture, solid and fluid phases respectively in the $x-$ direction; T_R, T_{Rf}, T_{Rs_k} are the depth-averaged turbulent Reynolds stresses for the fluid-solid mixture, fluid and solid phases in the $x-$ direction; T_μ, $T_{\mu f}$, $T_{\mu s_k}$ are the depth-averaged viscous stresses for the fluid-solid mixture, fluid and solid phases respectively in the $x-$ direction; $F_{s_k f}$ is the size-specific depth-averaged interphase interaction force; F_{s-s_k} is the size-specific depth-averaged particle-particle interaction drag force, which is exerted on sediment phase k by the other constituents of solid phase and $\sum(F_{s-s_k})=0$; $F_k=E_k-D_k$ is the size-specific net flux of sediment exchange between the flow and the bed, and $F_T=\sum F_k$, where E_k and D_k are the size-specific sediment entrainment and deposition fluxes respectively; h_a is the thickness of the active layer, f_{ak} is the fraction of the k th size sediment in the active layer and $\sum f_{ak}=1$; $\xi=z_b-h_a$ is the elevation of the bottom surface of the active layer; and f_{Ik} is the fraction of the k th size sediment in the interface between the active layer and the substrate layer and $\sum f_{Ik}=1$. For multi grain sizes, the widely used active layer formulation due to Hirano (1971), Eq. (8), is adopted to resolve bed grain size stratigraphic evolution. According to Hoey and Ferguson (1994), $h_a=2d_{84}$, where d_{84} is the particle size at which 84% of the sediments are finer. The complete governing equations for single-sized sediment transport can be obtained easily if $N=1$ in Eqs. (1-8).

Physically, there is no any real momentum exchange involved in the mass exchange between the flow and the bed, as highlighted by Cao et al. (2017). This is certainly justified because the flow momentum would not change as the sediment (and water) entrained from the static bed does not have any momentum initially. Likewise, the flow momentum does not vary due to the sediment deposited into the bed (Cao et al. 2017). Actually, this proposition has been correctly manifested in models for fluvial processes (e.g., Cao et al. 2004; Wu 2007) and also for earth surface flows such as debris flows (Bridge and Demicco 2008), as demonstrated by Eqs. (2), (4) and (6).

In summary, the model equations of the present depth-averaged two-phase model for fluvial sediment-laden flows over erodible beds can be derived from the conservation laws under the

framework of shallow water hydrodynamics, including the complete mass and momentum conservation equations for the fluid-solid mixture (Eqs. 1 and 2), the size-specific mass and momentum conservation equations for the solid phase (Eqs. 3 and 4), the mass and momentum conservation equations for the fluid phase (Eqs. 5 and 6), the global mass conservation equation for the sediments in the bed (Eq. 7) and the size-specific mass conservation equation for the sediments in the active layer of the bed surface (Eq. 8).

Indeed, the mass and momentum conservation equations for the fluid-solid mixture can be derived by adding their counterparts for the fluid and solid phases respectively. Specifically, Eq. (1) is the sum of Eqs. (3) and (5), and Eq. (2) is obtained by adding Eq. (4) to Eq. (6). Therefore, two of the three governing equation systems for the fluid-solid mixture (Eqs. 1-2), the solid phase (Eqs. 3-4) and the fluid phase (Eqs. 5-6) are independent numerically and can be used to formulate the mathematical model for fluvial sediment-laden flows. Accordingly, there are two distinct options available for numerical solution of the governing equations of the present two-phase model. Specifically, one concerns the equations for the fluid and solid phases respectively, while the other pertains to the equations for the fluid-solid mixture and solid phase. However, when the former alternative is used, the exact roots of the characteristic polynomial equations cannot be readily derived, even for the relatively simple case of single-sized sediment, i.e., $N=1$. Specifically, when the second-order terms are not present, the eigenvalues may become complex conjugate, leading to hyperbolicity loss (Pelanti et al. 2008; Pudasaini 2012). In this case, complexities arisein terms of numerical algorithm selection and boundary condition implementation. In contrast, the latter approach is certainly more attractive because the system composed of the equations for the fluid-solid mixture and solid phase (when the second-order terms are not present) is hyperbolic and thus the real and distinct eigenvalues can be derived straightforward. In accordance, the eigenvalues are:

$$\lambda_{m1,2}=U_m\pm\sqrt{gh} \tag{9a}$$

$$\lambda_{sk\,3,4}=U_{sk}\pm\sqrt{0.5(\rho_m/\rho_s)gh} \tag{9b}$$

where λ_m and λ_{sk} are the eigenvalues related to the motion of the fluid-solid mixture and solid phase respectively. Therefore, in the present study, the governing equation systems for the fluid-solid mixture (i.e., Eqs. 1-2) and the solid phase (i.e., Eqs. 3-4) along with the bed deformation equation (Eq. 7) and the active layer equation (Eq. 8) are solved numerically.

2.2. Comparisons with existing models

Physically, the present model represents a step forward as compared to the previous models for fluvial flows over erodible beds. Table 1 compares the key physical factors included in the present and previous models. Briefly, compared to existing depth-averaged two-phase models (e.g., Di Cristo et al. 2016), the present model is extended due to the incorporation of multi grain sizes, which reflects the real fluvial sediment-laden flows better than those models assuming a single size class. In comparison with the quasi single-phase mixture models, the depth-averaged velocities of the size-specific sediment phase are numerically resolved by virtue of the momentum conservation equation, one for each sediment size group, thus the interphase and particle-particle interactions are explicitly represented. Additionally, a single sediment transport equation is used for modelling bed load and suspended load simultaneously in the present study and quasi single-phase mixture models by Qian et al. (2015), while separate equations are solved for estimating bed load and suspended load sediment transport respectively in Di Cristo et al. (2016). The present approach is appropriate as it can not only ensure the smooth transition of sediment variables between bed load and suspended load for each size group, but also simplify the accounting of sediment and speed the computation (Greimann et al. 2008).

Indeed, under certain premises, the present two-phase model can degenerate into the traditional depth-averaged quasi single-phase mixture models (e.g., Qian et al. 2015). Briefly, modification coefficient $\beta_k = U_{sk}/U_m$ is introduced to estimate the velocity discrepancy between the size-specific sediment phase and the water-sediment mixture flow. Physically similar parameters have been proposed by Wu et al. (2006) and Greimann et al. (2008), suggesting $\beta_k \leq 1$. Introducing β_k in the model equations is physically justified, as the depth-averaged mean longitudinal velocity of bed load

is appreciably lower than that of the flow (Chien and Wan 1999), while for suspended load sediment, the value of β_k is generally set to be unity as suspended sediment transport has nearly the same depth-averaged longitudinal velocity as the water-sediment mixture. In line with this status, Eq. (4) is not needed and thus the remaining equations (i.e., Eqs. 1, 2, 3, 5, 7 and 8) become the same as those of the quasi single-phase mixture model (e.g., Qian et al. 2015) when the second-order terms are not present. For bed load sediment, β_k can be empirically determined by (Greimann et al. 2008)

$$\beta_k = \frac{U_{sk}}{U_m} = \frac{U_*}{U_m}\frac{1.1(\theta_k/0.047)^{0.17}[1-\exp(-5\theta_k/0.047)]}{\sqrt{0.047}} \tag{10}$$

where U_* is the bed shear velocity; $\theta_k = U_*^2/(sgd_k)$ is the size-specific Shields parameter with the specific gravity of sediment $s = (\rho_s - \rho_f)/\rho_f$.

Table 1 Comparisons of key physical factors included in the present and previous models.

	Physics	Implication	Indication	Two-phase models		Quasi single-phase mixture models
				Present model	Di Cristo et al. (2016)	Qian et al. (2015)
1	Multi grain sizes	Resolve size-specific motions	$N>1$	√	×	√
2	Interphase interaction	Represent relative motion of fluid and solid phases	$F_{s_k f}$	√	√	√ (Empirical Relationship)
3	Particle-particle interaction	Represent relative motion of grains	F_{s-s_k}	√	×	√ (Empirical Relationship)
4	Mass exchange between the flow and the bed	Represent flow-bed interaction	F_k	√	√	√
5	Turbulent Reynolds stresses	Represent fluid and solid turbulence	T_{Rf} and T_{Rs_k}	√	×	×

2.3. Model closures

To close the governing equations of the present depth-averaged two-phase model, a set of relationships have to be introduced to determine the bed shear stresses, sediment exchange fluxes, in addition to interphase and particle-particle interaction forces and turbulent Reynolds stresses.

2.3.1. Bed shear stresses

In general, boundary resistances of unsteady and non-uniform flows are substantially different from those of steady and uniform flows. When sediment transport is involved, this is more pronounced as morphological changes are generated. However, to date, there are no generally applicable relationships available to represent the boundary resistances for the fluid and solid phases in fluvial sediment-laden flows. Empiricism is inevitably introduced in terms of the bed shear stress estimation, which is common to all models for fluvial sediment-laden flows. The conventional practice in two-phase flow modeling (e.g., Greco et al. 2012; Di Cristo et al. 2016), in which the total bed shear stress for the fluid-solid mixture is separated into the respective bed shear stress exerted on the fluid and solid phases, is followed in the present study

$$\tau_b = \tau_{fb} + \sum(\tau_{s_k b}) \tag{11}$$

The solid phase resistance is determined by the Coulomb friction law (Savage and Hutter 1989), which expresses the collinearity of shear stress and normal stress through a friction coefficient $\tan\delta$. Following this practice, the bed shear stress exerted on the solid phase is given as follows,

$$\tau_{s_k b} = \rho_s g h_{sk} \tan\delta \hat{m}_b \,\mathrm{sgn}(U_{sk}) \tag{12a}$$

where $\hat{m}_b = \sqrt{1+(\partial z_b/\partial x)^2}$. Separately, the resistance relationship initially developed for steady and uniform flows, which is usually based on the Manning's equation, is employed to determine the fluid bed resistance.

$$\tau_{fb} = \rho_f g h_f \frac{n^2 U_f^2}{h_f^{4/3}} \hat{m}_b \tag{12b}$$

where n is the Manning roughness parameter. In the present study, the roughness of flume is directly used as the Manning roughness.

2.3.2. Sediment exchange between the flow and the bed

Generally, there are two distinct mechanisms involved in sediment exchange between the flow and the bed, i.e., bed sediment entrainment due to turbulence and sediment deposition by gravitational action, though sediment particle-particle interactions may modify the exchange to some extent. In terms of the determination of the entrainment and deposition fluxes, it continues to be one of the pivotal components of computational models for sediment transport and morphological evolution. However, current formulations hinge upon a series of premises. Here the conventional practice in fluvial hydraulics is followed in the present study (Wu 2007). The deposition flux can be practically determined due to the local near-bed sediment concentration and settling velocity. To specify the entrainment fluxes, one of the most widely used approaches is followed, which assumes that entrainment always occurs at the same rate as it does under capacity regime. In capacity conditions, the entrainment flux is equal to the deposition flux. Therefore, bed sediment entrainment flux can be computed by using near-bed sediment concentration at capacity and settling velocity. Accordingly, the entrainment and deposition fluxes are estimated by

$$E_k = \alpha_k \omega_k C_{ek}\,,\ D_k = \alpha_k \omega_k C_k \tag{13a, b}$$

where ω_k is the settling velocity of the k th grain size calculated using Zhang's formula (Zhang and Xie 1993),

$$\omega_k = \sqrt{(13.95\frac{\nu_{\mu f}}{d_k})^2 + 1.09sgd_k} - 13.95\frac{\nu_{\mu f}}{d_k} \tag{14}$$

where $\nu_{\mu f}$ is kinematic viscosity of the fluid phase; α_k is an empirical parameter representing the difference between the near-bed sediment concentration C_{bk} and the depth-averaged sediment concentration C_k. Here a unified and constant α_k is used and estimated by calibration in the

computation (Qian et al. 2015). The size-specific sediment concentration C_{ek} at capacity is computed as

$$C_{ek} = A_k q_k / (hU_m) \tag{15a}$$

where q_k is the size-specific transport rate at capacity regime, which is calculated by Wu formula (Wu 2007); A_k is the areal exposure fraction of k th sediment on the bed surface given by Parker (1991a, b) as below

$$A_k = \frac{f_{ak} / \sqrt{d_k}}{\sum (f_{ak} / \sqrt{d_k})} \tag{15b}$$

Wu (2007) suggested that each sediment size is transported as bed load and suspended load at the same time. Therefore, sediment transport rate of any size fraction can be determined as

$$\frac{q_k}{\varphi_k \sqrt{s g d_k^3}} = 0.0053 \left[(\frac{n'}{n_b})^{1.5} \frac{\tau_b}{\tau_{ck}} - 1 \right]^{2.2} + 0.0000262 \left[(\frac{\tau}{\tau_{ck}} - 1) \frac{U_m}{\omega_k} \right]^{1.74} \tag{15c}$$

where ϕ_k is the modification coefficient; $n' = d_{50}^{1/6} / 20$ is the Manning roughness corresponding to grain resistance; τ is the shear stress at channel cross-section; τ_{ck} is the critical shear stress for incipient motion of bed material, approximated by $\tau_{ck} = 0.03 \gamma_k (\rho_s - \rho_f) g d_k$ with γ_k representing the correction factor accounting for the hiding and exposure mechanisms in multi grain sizes of sediments (Wu 2007). It is also noted that Eq. (13a) is applicable when there is sufficient sediment supply from the bed. Otherwise, the sediment entrainment flux vanishes where the bed is made of rigid material (e.g., steel or concrete) and is locally non-erodible. The following relation is employed to evaluate f_{Ik} (Hoey and Ferguson 1994; Toro-Escobar et al. 1996)

$$f_{Ik} = \begin{cases} f_{sk} & \partial \xi / \partial t \le 0 \\ \varphi C_k / C_T + (1 - \varphi) f_{ak} & \partial \xi / \partial t > 0 \end{cases} \tag{16}$$

where f_{sk} is the fraction of the k th size sediment in the substrate layer; φ is the empirical weighting parameter.

2.3.3. Interaction force

The interphase interaction force mainly includes drag force, virtual (added) mass force and lift force. In general, the latter two forces can be ignored in shallow water hydrodynamic models (e.g., Pitman and Le 2005; Pelanti et al. 2008; Greco et al. 2012; Di Cristo et al. 2016), except the two-phase model for debris flows by Pudasaini (2012), which especially include the virtual mass force. Indeed, the effect of the virtual mass force is negligible according to the numerical results in Pudasaini (2012). The interphase drag force F_{Dk} can be expressed as below

$$F_{Dk} = \rho_f D_{rk} h(U_f - U_{sk}) \tag{17a}$$

where D_{rk} is the drag function and can be determined on the base of the drag correlation of Gidaspow (1994)

$$D_{rk} = \begin{cases} 150\dfrac{C_k^2 \nu_{\mu f}}{(1-\sum C_k) d_k^2} + \dfrac{7}{4}\dfrac{C_k}{d_k}\left|U_f - U_{sk}\right| & if\ C_k > 0.2 \\ \dfrac{3}{4} c_d(\mathrm{Re}_k)\dfrac{(1-\sum C_k) C_k}{d_k}(1-\sum C_k)^{-2.65}\left|U_f - U_{sk}\right| & if\ C_k \le 0.2 \end{cases} \tag{17b}$$

where the drag coefficient $c_d(\mathrm{Re}_k)$ is given by

$$c_d = \begin{cases} \dfrac{24}{\mathrm{Re}_k}(1.0 + 0.15\mathrm{Re}_k^{0.687}) & if\ \mathrm{Re}_k < 1000 \\ 0.44 & if\ \mathrm{Re}_k \ge 1000 \end{cases} \tag{17c}$$

where $\mathrm{Re}_k = C_f \left|U_f - U_{sk}\right| d_k / \nu_{\mu f}$ is the size-specific Reynolds number of the flow, $\nu_{\mu f}$ is kinematic viscosity of fluid phase.

Gray and Chugunov (2006) suggested that particle-particle interaction drag force included a linear velocity-dependent drag force, a particle-particle surface interaction force and a remixing force. By depth-averaging, the size-specific interaction drag

F_{s-s_k} can be formulated as follows:

$$F_{s-s_k} = \int_{z_b}^{z_b+h} f_{s-s_k} dz = \frac{1}{2} C_T \rho_m g h \frac{\partial}{\partial x}(\frac{C_k}{C_T}) - \rho_s \frac{C_k}{C_T} c_{sd}(U_{sk} - \bar{U}_s)h - \rho_s \nu_d h \frac{\partial}{\partial x}(\frac{C_k}{C_T}) \quad (18)$$

where $\bar{U}_s = \sum(C_k U_{sk})/C_T$ is the depth-averaged mean sediment velocity, c_{sd} is the liner drag coefficient and ν_d is the linear diffusive coefficient. In the present study, c_{sd} = 6.3 s^{-1}, ν_d = 1.26 ×10^{-5} m^2 s^{-2} following Hill and Tan (2014).

2.3.4. Turbulence modelling

The depth-averaged turbulent Reynolds stresses for the fluid and solid phases, which explicitly describe their respective contributions to the fluid and solid momentums, can be readily derived by transforming the basic three-dimensional two-phase equations through Reynolds averaging procedure. Although the depth-averaged turbulent Reynolds stresses are generally negligible in fluvial sediment-laden flow modelling, it is sensible to incorporate its effect for wide applicability.

The depth-averaged turbulent Reynolds stresses for the fluid and solid phases, including $T_{Rf} = -\rho_f \overline{U_f'^2}$, $T_{Rs_k} = -\rho_s \overline{U_{sk}'^2}$, are determined following Boussinesq's eddy-viscosity concept (Rastogi and Rodi 1978; Chauchat and Guillou 2008)

$$T_{Rf} = -\rho_f \overline{U_f'^2} = \rho_f (2\nu_{tf} \frac{\partial U_f}{\partial x} - \frac{2}{3} k_f) \quad (19a)$$

$$T_{Rs_k} = -\rho_s \overline{U_{sk}'^2} = \rho_s (2\nu_{ts_k} \frac{\partial U_{sk}}{\partial x} - \frac{2}{3} k_{s_k}) \quad (19b)$$

where k_f , k_{s_k} are the depth-averaged turbulent kinetic energies for the fluid and solid phases respectively; ν_{tf} , ν_{ts_k} are the depth-averaged eddy viscosities of the fluid and solid phases.

The depth-averaged viscous stresses for the fluid and solid phases respectively are determined by

$$T_{\mu f} = 2\rho_f \nu_{\mu f} \frac{\partial U_f}{\partial x} \quad (20a)$$

$$T_{\mu s_k} = 2\rho_s \nu_{\mu s_k} \frac{\partial U_{sk}}{\partial x} \tag{20b}$$

where $\nu_{\mu s_k}$ is the viscosity related to inter-granular stress, which can be evaluated based on Ahilan and Sleath (1987) formula

$$\nu_{\mu s_k} = 1.2 \frac{\rho_f}{\rho_s} [(\frac{C_k^{\max}}{C_k})^{1/3} - 1]^{-2} \nu_{\mu f} \tag{21}$$

where $C_k^{\max}$ is the depth-averaged size-specific maximum sediment volumetric concentration. In the present study, $C_k^{\max}$ is assumed to be equal to $C_{critical}$, the volume fraction of random close packing (RCP), which is defined as the densest amorphous packing of rigid particles in the broad field of physics. The practice of using unified value for $C_k^{\max}$ demonstrates that the sediment concentration of any size group can reach the volume fraction of random close packing theoretically. And it is reasonable to assume $T_R = \sum (C_k T_{Rs_k}) + C_f T_{Rf}$, $T_\mu = \sum (C_k T_{\mu s_k}) + C_f T_{\mu f}$.

Here the fluid turbulence is modelled by the turbulent kinetic energy - dissipation rate model, i.e., $k_f - \varepsilon_f$ model, where ε_f is the depth-averaged dissipation rate of turbulent kinetic energy, while the turbulent Reynolds stress for the solid phase is modelled by a closure model originating from the kinetic theory of granular flows (Jenkins and Richman 1985), in which two transport equations are solved respectively for the turbulent kinetic energy for the solid phase (k_{s_k}) and the fluid particle covariance ($k_{s_k f}$).

Specifically, the fluid turbulent stress is determined by the standard depth-averaged $k_f - \varepsilon_f$ turbulence model proposed by Rastogi and Rodi (1978) along with a modified component accounting for the influence of particles (Simonin and Viollet 1990). Equations for the depth-averaged turbulent kinetic energy and dissipation rate of turbulent kinetic energy of the fluid phase are written as follows:

$$\frac{\partial h_f k_f}{\partial t} + \frac{\partial h_f U_f k_f}{\partial x} = \frac{\partial}{\partial x} (\frac{\nu_{tf}}{\sigma_k} h_f \frac{\partial k_f}{\partial x}) + h_f (P_{kf} + P_{kfb} - \varepsilon_f) + \Pi_{k_f} \tag{22}$$

$$\frac{\partial h_f \varepsilon_f}{\partial t} + \frac{\partial h_f U_f \varepsilon_f}{\partial x} = \frac{\partial}{\partial x}\left(\frac{\nu_{tf}}{\sigma_\varepsilon} h_f \frac{\partial \varepsilon_f}{\partial x}\right) + h_f\left(C_{\varepsilon 1} P_{kf} - C_{\varepsilon 2}\varepsilon_f + P_{\varepsilon fb}\right) + \Pi_{\varepsilon_f} \tag{23}$$

where P_{kf} is the production of turbulence due to the longitudinal velocity gradients, defined as $P_{kf} = 2\nu_{tf}(\partial U_f / \partial x)^2$; P_{kfb} and $P_{\varepsilon fb}$ are the production terms from non-uniformity of vertical profiles of the fluid phase, related to the fluid friction velocity u_{f*} by $P_{kfb} = c_{ff}^{-1/2} u_{f*}^3 / h_f$ and $P_{\varepsilon fb} = C_\Gamma C_{\varepsilon 2} C_\mu^{1/2} c_{ff}^{-3} u_{f*}^4 / h_f^2$, where $c_{ff} = g n^2 / h_f^{1/3}$ and $u_{f*} = \sqrt{\tau_{fb}/\rho_f}$ (Rastogi and Rodi 1978). The kinematic turbulent viscosity of the fluid phase ν_{tf} is defined as $\nu_{tf} = C_\mu k_f^2 / \varepsilon_f$ (Rastogi and Rodi 1978). C_μ, C_Γ, $C_{\varepsilon 1}$, $C_{\varepsilon 2}$, σ_k, σ_ε are empirical constants (Rastogi and Rodi 1978).

In the Eqs. (22 and 23), the terms $\prod_{k_f}$ and $\prod_{\varepsilon_f}$ represent the influence of particles, they are defined as follows (Simonin and Viollet 1990):

$$\Pi_{k_f} = \sum [C_k \frac{h_f}{T_{pr_k}}(-2k_f + k_{s_k f} + U_{dk} U_{rk})] \Big/ C_T \,,\ \Pi_{\varepsilon_f} = C_{\varepsilon 3} \frac{\varepsilon_f}{k_f} \Pi_{k_f} \tag{24a, b}$$

where T_{pr_k} is the particle relaxation time and defined as $T_{pr_k} = \frac{4 d_k \rho_s}{3 \rho_f C_D |U_r|} C_f^{-2.65}$ (Enwald et al. 1996), and $U_{rk} = U_f - U_{sk} - U_{dk}$ is the mean relative velocity between fluid and solid phases, and U_{dk} represents the correlation between the turbulent velocity of the fluid phase and the spatial distribution of the solid phase. This term, called the drift velocity, represents the dispersion of particles by the large scale of the turbulent motion in the fluid phase, large with respect to the particle diameter (Simonin and Viollet 1990). According to Deutsch and Simonin (1991), the drift velocity can be defined as

$$U_{dk} = \frac{T_{fp_k}^t k_{s_k f}}{3}\left(\frac{1}{C_k}\frac{\partial C_k}{\partial x} - \frac{1}{C_f}\frac{\partial C_f}{\partial x}\right) \tag{25}$$

where $T_{fp_k}^t$ is the fluid particle turbulent time scale and expressed as $T_{fp_k}^t = \gamma_{sk} T_f^t$, and

$\gamma_{sk} = [1 + C_\beta \sqrt{3|U_{rk}|^2 / 2k_f}]^{-1/2}$; the coefficient $C_\beta = 1.8 - 1.35\cos^2\alpha$, depending on the angle α between flow direction and relative mean velocity; T_f^t is the time scale of large eddies $T_f^t = 1.5 C_\mu k_f / \varepsilon_f$. All these constants in turbulence model for the fluid phase, except $C_{\varepsilon 3}$, have the same values as those in standard single-phase $k_f - \varepsilon_f$ model (Launder and Spalding 1974). $C_{\varepsilon 3}$ is included in the interaction term for dissipation and has been determined empirically from turbulent gas particle jet flows (Elghobashi and Abou-Arab 1983).

The $k_{s_k} - k_{s_k f}$ turbulence model for the solid phase originates from the framework of the kinetic theory of granular flow (Jenkins and Richman 1985). The $k_{s_k} - k_{s_k f}$ model is based on two transport equations, one for the turbulent kinetic energy of the solid phase k_{s_k} (Eq. 26), and one for the fluid particle velocity covariance, $k_{s_k f}$ (Eq. 27) (Simonin 1991). By depth-averaging the equations proposed by Simonin (1991), the $k_{s_k} - k_{s_k f}$ model for solid phase turbulence is expressed as follows

$$\frac{\partial h_{sk} k_{s_k}}{\partial t} + \frac{\partial h_{sk} U_{sk} k_{s_k}}{\partial x} = \frac{\partial}{\partial x}\left(h_{sk} D_{sk} \frac{\partial k_{s_k}}{\partial x}\right) - h_{sk} \frac{1 - e^2}{3 T_s^c} k_{s_k} + 2 h_{sk} \nu_{ts_k} \left(\frac{\partial U_{sk}}{\partial x}\right)^2 + h_{sk} P_{ks_k b} - \frac{h_{sk}}{T_{pr_k}} (2 k_{s_k} - k_{s_k f}) \tag{26}$$

$$\frac{\partial h_{sk} k_{s_k f}}{\partial t} + \frac{\partial h_{sk} U_{sk} k_{s_k f}}{\partial x} = \frac{\partial}{\partial x}\left(h_{sk} \frac{\nu_{ts_k f}}{\sigma_{s_k f}} \frac{\partial k_{s_k f}}{\partial x}\right) - h_{sk} \varepsilon_{s_k f} + h_{sk} \nu_{ts_k f} \left(\frac{\partial U_{sk}}{\partial x} + \frac{\partial U_f}{\partial x}\right)^2 + h_{sk} (P_{ks_k b} + P_{kfb}) - \frac{h_{sk}}{T_{pr_k}} ((1 + X_{s_k f}) k_{s_k f} - 2 X_{s_k f} k_{s_k} - 2 k_f) \tag{27}$$

where $\sigma_{s_k f}$ is an empirical constant and $\sigma_{s_k f}$ = 1.0 following Chauchat and Guillou (2008); $D_{sk} = K_{sk}^t + K_{sk}^c$ and K_{sk}^t, K_{sk}^c represent the turbulent and collisional diffusivities respectively, which can be empirically determined as below (Chauchat and Guillou 2008)

$$K_{sk}^{t}=\frac{\frac{1}{3}T_{fp_k}^{t}k_{s_k f}+\frac{5}{9}T_{pr_k}\frac{2}{3}k_{s_k}(1+C_k g_o\phi_c)}{1+\frac{5}{9}T_{pr_k}\frac{\varsigma_c}{T_{s_k}^{c}}} \tag{28}$$

$$K_{sk}^{c}=C_k g_o(1+e)(\frac{6}{5}K_{sk}^{t}+\frac{4}{3}d_k\sqrt{\frac{2k_{s_k}}{3\pi}}) \tag{29}$$

where $\phi_c=3(1+e)^2(2e-1)/5$ and $\varsigma_c=(1+e)(49-33e)/100$; e is the restitution coefficient of binary collisions and e= 0.9 according to Chauchat and Guillou (2008); g_0 is the radial distribution function which accounts for the increase in the probability of collisions when the sediment concentration increases. Here the radial distribution function suggested by Torquato (1995) is used.

$$g_0=\begin{cases}\dfrac{(1-C_k/2)}{(1-C_k)^3} & if\ 0<C_k<C_{freeze}\\ g_{freeze}\dfrac{(C_{critical}-C_{freeze})}{(C_{critical}-C_k)} & if\ C_{freeze}<C_k<C_{critical}\end{cases} \tag{30}$$

where $g_{freeze}=(1-C_{freeze}/2)/(1-C_{freeze})^3$ denotes the contact value of the radial distribution function at the freezing packing fraction C_{freeze}, which is closely related to $C_{critical}$ (Torquato and Stillinger (2007). Theoretically, the volume fractions of random close packing and freezing packing are both influenced by the grain size distribution and relative grain size of sediment mixture (Torquato and Stillinger 2010; Desmond and Weeks 2014). However, to date, there are no universally applicable formula for determining the volume fraction of random close packing, as previous studies in this regard (e.g., Torquato and Stillinger 2010; Desmond and Weeks 2014) are generally based on the presumed function for particle size distribution. Moreover, as illustrated by Desmond and Weeks (2014), the value of random close packing fraction varies in a narrow range of 0.64 to 0.70. In this connection, the effects of particle size distribution on the fraction of random close packing can be actually neglected in numerical computation. Therefore, following Torquato (1995), the values of the random close packing fraction ($C_{critical}$) and freezing packing fraction (C_{freeze}) are assumed to be constant and taken to be 0.64 and 0.49 respectively. $T_{s_k}^{c}$ is the inter-particle collision time scale and is

given in the framework of the kinetic theory of granular flows as $T_{s_k}^c = \frac{d_k}{24 g_o C_k}\sqrt{(3\pi)/(2k_{s_k})}$. $P_{ks_k b}$ is the production term from non-uniformity of vertical profiles of the solid phase, related to the friction velocity $u_{s_k *}$ by $P_{ks_k b} = c_{fs_k}^{-1/2} u_{s_k *}^3 / h_{sk}$, where $c_{fs_k} = \tau_{s_k b}/\rho_s U_{sk}^2$ and $u_{s_k *} = \sqrt{\tau_{s_k b}/\rho_s}$. And the dissipation rate $\varepsilon_{s_k f}$, is given by $\varepsilon_{s_k f} = k_{s_k f}/T_{fp_k}^t$ and is a function of fluid particle velocity covariance $k_{s_k f}$ and the fluid particle turbulent time $T_{fp_k}^t$; $X_{s_k f} = C_k \rho_s / C_f \rho_f$. In $k_{s_k} - k_{s_k f}$ model, the solid phase turbulent viscosity ν_{ts_k} is defined as (Chauchat and Guillou 2008)

$$\nu_{ts_k} = [\nu_{ts_k f} + \frac{1}{3} T_{pr_k} k_{s_k}][1 + \frac{\sigma_{sk} T_{pr_k}}{2T_{s_k}^c}]^{-1} \tag{31}$$

where the turbulent fluid particle viscosity $\nu_{ts_k f} = k_{s_k f} T_{fp_k}^t / 3$; σ_{sk} is an empirical coefficient with the value of 1.0 (Chauchat and Guillou 2008). The values of the coefficients involved in the turbulence models for both the fluid and solid phases are summarized in Table 2.

Table 2 Coefficients in the turbulence models.

$k_f - \varepsilon_f$	C_μ	$C_{\varepsilon 1}$	$C_{\varepsilon 2}$	$C_{\varepsilon 3}$	σ_k	σ_ε	C_Γ
model	0.09	1.44	1.92	1.2	1.0	1.3	3.6
$k_{s_k} - k_{s_k f}$	$\sigma_{s_k f}$	σ_{sk}	e	C_{freeze}	$C_{critical}$		
model	1.0	1.0	0.9	0.49	0.64		

The depth-averaged two-phase model equations along with the model closures have been presented above. Physically, as compared to existing depth-averaged two-phase models (e.g., Greco et al. 2012; Di Cristo et al. 2016), the present model represents a step forward in two-phase modeling of fluvial processes over erodible beds by explicitly incorporating multi grain sizes of sediments. The present depth-averaged two-phase model is solved by the numerical algorithm adapted from Cao et al. (2015a), which is described in Supplementary B.

3. Computational case studies

A series of test cases are resolved to evaluate the present depth-averaged two-phase model (TPE), including comparisons with the quasi single-phase mixture models (Qian et al. 2015). The test cases concern (1) the refilling of a dredged trench documented by van Rijn (1986), (2) an extended case of trench refilling presented by Armanini and Di Silvio (1988), (3) bed aggradation due to sediment overloading (Seal et al. 1997), and (4) flood flows due to landslide dam failure (Cao et al. 2011) respectively. In addition, the case concerning bed degradation due to flash floods (Reid et al. 1995) is also revisited (Supplementary C), which further substantiates the applicability of the present TPE model. In this regard, it is noted that more test cases involving relatively higher sediment concentrations are required to further demonstrate the present model's advantages over quasi singe-phase models.

To evaluate the discrepancy between the numerical solution and the measured data, the non-dimensional discrepancy is defined based on the L^1 norm

$$L^1_{stage} = \frac{\sum abs(\eta_i - \hat{\eta}_i)}{\sum h_i} \tag{32}$$

$$L^1_{bed} = \frac{\sum abs(\Delta z_{bi} - \Delta \hat{z}_{bi})}{\sum \Delta z_{bi}} \tag{33}$$

where L^1_{stage} and L^1_{bed} are L^1 norms for stage and bed deformation depth respectively. The bed deformation depth is defined by $\Delta z_b = z_b - z_b(t=0)$, and $\hat{\eta}$, $\hat{z}_b$ are measured stage and bed deformation, whilst η, z_b are the stage and bed deformation computed from a numerical solution.

In the present work, a fixed uniform mesh is used. The friction angle $\delta = 32^o$. The empirical weighting parameter ϕ, which was suggested to vary between 0.61 and 0.81 based on the sediment size (Toro-Escobar et al. 1996), is calibrated to be 0.65 for the present computational cases. The values of the other common parameters are $\rho_f = 1000$ kg/m^3, $\rho_s = 2650$ kg/m^3, and $g = 9.8$ m^2/s. Unless otherwise specified, the bed porosity is estimated by $p = 0.13 + 0.21/(1000 \times d_{50} + 0.002)^{0.2}$ (Wu

and Wang 2006), where d_{50} is the particle size at which 50% of the sediments are finer. The values of the modification coefficient ϕ and the empirical parameter α need to be calibrated based on measured data. The modelling parameters are listed in Table 3. Notably, the modelling parameters used in the TPE model (Table 3) are the same as those in the quasi single-phase mixture model by Qian et al. (2015, Table 2). Theoretically, in this instance, the superiority of the TPE model over the quasi single-phase mixture model can be demonstrated when the TPE model performs better.

Table 3 List of the parameter value.

Case	Cr	Δx (m)	ϕ	α
1	0.9	0.25	2.3	18.0
2	0.9	0.1	0.5	25.0
3	0.9	0.2	1.0	20.0
4	0.9	0.04	5.0	5.0

3.1. Refilling of a dredged trench (Case 1)

First, the present two-phase model was applied to a flume experiment carried out at Delft Hydraulics Laboratory, concerning the refilling of a dredged trench. A gentle-sided (1:10) trench with an initial depth of 0.15 m was set up in a flume of dimensions 30×0.5×0.7 m. A constant unit inflow discharge of 0.2 m^2/s was specified at the inlet, with the mean flow depth and velocity stabilizing at 0.39 m and 0.51 m/s respectively. The bed was composed of fine sand (0.16 mm) with the setting velocity of 0.013 m/s. The Manning roughness n is 0.011 $s/m^{1/3}$. During the experiment, equilibrium sediment transport was maintained at the inlet boundary, thus the corresponding equilibrium rate was 0.03 kg/m/s and the sediment concentration by weight at the cross section was 0.1508 kg/m^3.

Fig. 1 shows the stage and bed profiles computed by the TPE model and the quasi single-phase mixture model by Qian et al. (2015) along with the measured bed data. The bed deformations are well reproduced by both models as compared to the measured data. The stage profiles from TPE model and quasi single-phase mixture model by Qian et al. (2015) are both rather smooth. Quantitatively, the values of the L_{bed}^1 norms of the TPE model and Qian et al. (2015) are similar (Table 4), while the TPE

model features a slight improvement. Fig. 2 illustrates the depth-averaged longitudinal velocity profiles of the water-sediment mixture, fluid (water) and sediment phase computed by the TPE model. It is shown that the sediment is transported as bed load because its depth-averaged longitudinal velocity is appreciably lower than the depth-averaged fluid velocity and the suspension index SI is larger than 2.6 (not shown), where $\mathrm{SI} = \omega/\kappa U_*$ and $\kappa = 0.4$, von Karman constant. In general, $\mathrm{SI} \geq$ 2.5 ensures that bed load sediment dominates over suspension. Yet as the sediment concentration is relatively low, the water-sediment mixture's velocity is approximately equal to the fluid velocity and thus the discrepancy between them is indistinguishable from Fig. 2.

Table 4 Values of L_{bed}^1 -norm of TPE model and Qian et al. (2015).

	$t =$ 7.5 h	$t =$ 15 h	Average
TPE (%)	8.27	2.62	5.44
Qian et al (2015) (%)	10.35	3.51	6.93

3.2. Extended case of dredged filling (Case 2)

To evaluate the capability of the TPE model in modelling non-uniform sediment transport and morphological evolution, an extended case of trench refilling designed by Armanini and Di Silvio (1988) is revisited. In this case, a trench of the rather steep side slope (1:3) was set up and the sediment mixture consisted of two fractions: d_1 = 0.075 mm (50%) and d_2 = 0.3 mm (50%). The unit inflow discharge was kept constant as 0.2 m^2/s.

Fig. 3 illustrates the computed stage and bed profiles at 7.5 h and 15 h from the TPE model and Qian et al. (2015), along with the bed profiles computed by quasi single-phase mixture model by Armanini and Di Silvio (1988). Seen from Fig. 3, rather limited differences in the bed profiles are observed for this case, featuring similar performances of the TPE model, Qian et al. (2015) and Armanini and Di Silvio (1988). The depth-averaged longitudinal velocity profiles of the water-sediment mixture, fluid and the size-specific sediment phases at 7.5 h and 15 h from the TPE model are illustrated in Fig. 4. Here the profiles of the depth-averaged mean sediment velocity $\bar{U}_s = \sum(U_{sk}C_k)/C_T$ are also included. The sediment phase with finer grain size (d_1 = 0.075 mm) exhibits as suspended load (suspension index $\mathrm{SI} <$ 0.5) and has nearly the same depth-averaged

longitudinal velocity as the water-sediment mixture and the fluid phase, whilst a marginal velocity lag can be observed. In contrast, the coarser grains (d_2 = 0.3 mm) are transported as bed load sediment because the depth-averaged velocity of the sediment phase is shown to be remarkably lower than that of the water-sediment mixture and the fluid phase, and suspension index SI is greater than 4.0. Similarly, due to the relatively low sediment concentration, indistinguishable velocity difference can be observed between the water-sediment mixture and the fluid phase. Notably, the larger the grain size, the smaller the depth-averaged sediment velocity. Although measured data is unavailable to quantitatively verify the computed results, this finding is qualitatively consistent with existing experimental observations (Wilcock 1997) and field data (Drake et al. 1988; Ferguson and Wathen 1998; Lenzi 2004), which further demonstrates the performance of the present model. In contrast, the velocity discrepancy among particles of different grain sizes cannot be resolved numerically by the depth-averaged quasi single-phase mixture model and by existing depth-averaged two-phase models based on a single size of sediments. Arguably, this is why it has not been reproduced numerically until the present work, although it has been observed for long.

3.3. Aggradation due to sediment overloading (Case 3)

Bed aggradation due to sediment overloading was performed at the St. Antony Fall Laboratory (Seal et al. 1997) in a flume of 45 m long and 0.305 m wide with a uniform slope of 0.002 (Fig. 5). A constant clear water inflow of 0.049 m^3/s was released at the inlet boundary, and a constant water level 0.4 m was maintained at the outlet boundary. Sediment mixture was fed into the flume manually at 1 m downstream of the headgate of the flume with a constant rate (Fig. 5), leading to the formation of a depositional wedge. Table 5 summarizes the grain size distribution of the fed sediment. Three runs of experiments were conducted. Here Run 1 was revisited to test the performance of the TPE model. The sediment feeding rate was 11.3 kg/min and was maintained for 16.8 h. The roughness is estimated as $n = [(Bn_b^{3/2} + 2hn_w^{3/2})/(B+2h)]^{2/3}$, where $n_b = 0.028$ $m^{-1/3}$ s and $n_w = 0.009$ $m^{-1/3}$ s are bed and wall roughness respectively. For this modelling exercise, the sediment input was treated as source terms in the governing Eqs. (1) and (3) in a similar way to Wu and Wang (2008) and Qian et al. (2015).

Besides, mass collapse was incorporated as it was observed frequently on the upstream side of the wedge during the experiments because its slope was steeper that the sediment repose angle (32º).

Fig. 6 illustrates the computed bed profiles at selected instants and final stage profile from TPE model and Qian et al. (2015) as compared to the measured data. In response to sediment feeding, the original clear water becomes over-loaded gradually, leading to the formation of a wedge with rather steep leading edge and the depositional front as well as their progressive propagation downstream. Seen from Fig. 6, the wedge-shaped bed profiles and the depositional front propagation are reproduced fairly well by both models, which are corroborated quantitatively by the values of L_{bed}^{1} (Table 6) and L_{stage}^{1} (Table 7). Also, seen from Tables 6 and 7, the TPE model features appreciable improvement in modelling performance. Fig. 7 shows the measured and computed characteristic grain sizes d_{10}, d_{50} and d_{90} of the substrate layer in the 0-5 hours and 5-10 hours timeline respectively, where d_{10}, d_{50} and d_{90} denote the particle size at which 10%, 50% and 90% of the sediment are finer respectively. As shown in Fig. 7, the general downstream fining at the bed surface in the longitudinal direction is well captured by the TPE model. Fig. 8 shows the depth-averaged longitudinal velocity profiles of the water-sediment mixture, fluid and selected size-specific sediment phases along with the profiles of the depth-averaged mean sediment velocity. Seen from Fig. 8, all the sediment phases exhibit as bed load because their depth-averaged longitudinal velocities are appreciably lower than the water-sediment mixture and fluid velocities and the suspension index SI are exclusively larger than 2.63. Similar to Cases (1) and (2) above, the velocity discrepancy between the water-sediment mixture and the fluid phase is indistinguishable because the volumetric sediment concentration is low. Moreover, the TPE model clearly resolve the phenomenon that the larger the grain size, the lower the depth-averaged sediment velocity.

Table 5 Grain size distribution of the fed sediment.

d_k (mm)	0.67	2.37	3.34	4.73	6.7	9.47	13.39	18.93	26.56	37.64	53.24	64
(%)	33.1	2.3	5.8	8.3	6.6	5.7	6.3	9.5	9.8	5.4	3.6	3.6

Table 6 Values of L^1_{bed} -norm of TPE model and Qian et al. (2015).

	$t = 2$ h	$t = 8$ h	$t = 16.8$ h	Average
TPE model (%)	3.53	8.95	5.68	6.05
Qian et al. 2015 (%)	6.47	9.14	4.96	6.85

Table 7 Values of L^1_{stage} -norm of TPE model and Qian et al. (2015).

	$t = 16.8$ h
TPE model (%)	5.60
Qian et al. 2015 (%)	8.87

3.4. Flood flows due to landslide dam failure

Here the present TPE model was further evaluated as applied to the modelling of flood flows due to landslide dam failure, in contrast to the general fluvial flows revisited above. A series of flume experiments on landslide dam breach and the resulting floods are documented by Cao et al. (2011). These experiments were carried out in a flume of dimensions 80 m×1.2 m×0.8 m (Fig. 9) and bed slope 0.001 and bed roughness $n = 0.012$ m$^{-1/3}$ s. A set of 12 automatic water-level probes was used to measure the stage hydrographs at 12 cross-sections along the flume. To demonstrate the performance of the model, a non-uniform sediment case with no initial breach, i.e., F- Case 16, is revisited here. In this case, the dam with a crest width of 0.2 m was initially 0.4 m high, located at approximately 41 m from the inlet of the flume. The initial upstream and downstream slopes of the dam were 1/4 and 1/5, respectively. The inlet flow discharge was 0.025 m^3/s. The initial static water depths immediately upstream and downstream of the dam were 0.054 m and 0.048 m respectively and a 0.15-m-high weir was installed at the outlet of the flume to hold the downstream water under the initial condition. The dam material was sediment mixture composed of the sand and gravel with the median diameter of 2.0 mm. According to the gradation curves, the mixture is separated here to two size fractions: $d_1 = 0.8$ mm (70%) and $d_2 = 5$ mm (30%).

In the experiments, the dams failed due to the erosion of the overtopping flow. When the dam failure commences, the flow upstream the dam recedes quickly. In contrast, the flow downstream the dam experiences three stages: the initial rising, subsequent gradual recession, and final stabilization.

These processes have been documented in details in Cao et al. (2011). Fig. 10 shows the computed stage hydrographs by TPE model and Qian et al. (2015) and the measured data at selected cross-sections. Specifically, the cross-sections CS 1, CS 5, CS 8 and CS 12 are located at 19 m, 40 m, 54 m and 73.5 m, respectively, from the inlet (Fig. 9). The former two cross-sections (CS 1 and CS 5) are upstream the dam, while the rest two (CS 8 and CS 12) are downstream the dam. It is seen from Fig. 10 that the stage hydrographs are well reproduced by both TPE model and Qian et al. (2015). Fig. 11 illustrates the stage and bed profiles from TPE model and Qian et al. (2015), along with the measured data for the stages. Shortly after the dam failure (e.g., $t =$ 670 s, 700 s and 730 s), the performances of both models are nearly the same. However, during the later period (i.e., $t =$ 900s), TPE model is demonstrated to be better than Qian et al. (2015) in reproducing bed deformation, as some oscillations are exhibited on bed profiles from Qian et al. (2015). Yet, it is premature to conclude if the oscillations stem from the empirical relationship for determining the sediment velocity embedded in the quasi single-phase mixture model. Thus, further investigations are necessary to qualitatively delimit the impacts of empirical formula for the sediment velocity on modelling fluvial sediment-laden flows. Moreover, the values of L^1_{stage} illustrated in Table 8 shows that the TPE model is relatively more close to the measured stage than Qian et al. (2015). Fig. 12 presents the computed depth-averaged longitudinal velocity profiles of the water-sediment mixture, fluid and sediment phases along with the profiles of the depth-averaged mean sediment velocity at selected instants. In contrast to the cases revisited above (Cases 1-3), appreciable velocity discrepancy between the water-sediment mixture and the fluid phase can be observed due to the existence of relatively high sediment concentrations (≈ 0.1) (Figs. 12 a and b). The two sediment fractions are both transported as bed load with the suspension index SI > 3.1 and the appreciable smaller depth-averaged velocities as compared to those of the water-sediment mixture and the fluid phase. Moreover, the larger the grain size, the slower the sediment fraction transports.

Table 8 Values of L^1_{stage}-norm of TPE model and Qian et al. (2015).

	$t =$ 670 s	$t =$ 700 s	$t =$ 730 s	$t =$ 900 s	Average

TPE model (%)	6.12	4.98	4.64	1.18	4.23
Qian et al. 2015 (%)	6.23	8.85	6.25	2.24	5.89

3.5. Discussion

3.5.1. Influences of turbulent Reynolds stresses

In relation to Cases 3 and 4, Figs. 13 and 14 respectively show the spatial distributions of $S_{T_{Rf}}/S_B$ and $S_{T_{Rs}}/S_B$ at specific instants, where $S_{T_{Rf}} = \partial hC_f T_{Rf}/\partial x$ and $S_{T_{Rs}} = \sum \partial hC_k T_{Rs_k}/\partial x$ represent the depth-averaged fluid and solid turbulent Reynolds stress terms, and $S_B = \mathrm{abs}(\tau_b)$ denotes the frictional term. It is seen from Figs. 13 and 14, the influence of the depth-averaged solid turbulent Reynolds stress $S_{T_{Rs}}$ can be neglected as the sediment concentration is sufficiently low. For Case 3, $S_{T_{Rf}}$ plays a minor role as the peak value of $S_{T_{Rf}}/S_B$ is less than 0.08, while for Case 4, the influence of $S_{T_{Rf}}$ is relatively greater with the maximum value of $S_{T_{Rf}}/S_B$ reaching 0.3. In general, the value of $S_{T_{Rf}}$ is negligible where the flow is gradually varied longitudinally, while it is relatively considerable where the flow is rapidly varied and clearly exhibits complex structure like hydraulic jump (Figs. 13 and 14).

3.5.2. CPU Runtime

The TPE model facilitates deeper insight into sediment-laden flows than the quasi single-phase mixture model. Yet, the CPU runtime of the TPE model relative to its counterpart of the quasi single-phase mixture model increases inevitably with the number of the size groups of the sediments, because a separate momentum conservation equation for each sediment size has to be solved. Table 9 lists the CPU runtime of TPE model relative to the counterpart of the quasi single-phase mixture model. Technically, a major concern arises from the great increase in computational cost, especially when the TPE model is applied for modeling natural large-scale fluvial processes, characterized by a broad

particle size-distribution. In this connection, the technique of adaptive mesh refining can be employed, which can efficiently save computational time by an order of magnitude (Huang et al. 2015).

Table 9 Relative CPU runtime.

Case	1	2	3	4
TPE	1.05	1.08	1.92	1.09

Overall the present two-phase model performs rather well in modelling fluvial sediment-laden flows, with appreciable improvement in modelling accuracy (Tables 4, 6, 7, 8) and an increase in computational cost (Table 9) as compared to quasi single-phase mixture model. Essentially, it is the physically enhanced capability rather than modelling accuracy or computational efficiency that distinguishes the present two-phase model from the quasi single-phase mixture model. In general, one of the most important strategies to enhance the quality of computational models for fluvial processes is to incorporate as much physics as possible and thereby minimize the assumptions. The present work is just one of the examples with respect to this philosophy, i.e., eliminating the empirical relationship for size-specific sediment velocities generic to quasi single-phase mixture models by applying the fundamental momentum conservation law for the sediment phase, one for each size group. To date, it remains unclear if such empirical approach is universally applicable for fluvial sediment-laden flows. Most importantly, the present TPE model reproduces the finding that the depth-averaged longitudinal sediment velocity decreases with the increase of grain size, which has been revealed for long by the existing experimental observations and field data but not yet resolved numerically by depth-averaged models. From this perspective, the advantage of the TPE model is obvious. It is appreciated that more modelling case studies with observed data are warranted to further demonstrate the superiority of the TPE model over quasi single-phase mixture model.

Extension of the present TPE model to two dimensions is warranted for field cases in natural river with complex and irregular topography. Then it should find wider applications in modelling fluvial sediment-laden flows over erodible beds.

4. Conclusions

A physically enhanced depth-averaged two-phase model is presented for fluvial sediment-laden flows over erodible beds. It is fully coupled and generally applicable, as the interactions among water flow, sediment and the bed and also among particles of different grain sizes are explicitly accounted for. It has been demonstrated to perform rather well when tested against a series of typical cases. Essentially, the present model reproduces the finding that the longitudinal sediment velocity decreases with the increase of grain size, which has been revealed for long by the existing experimental observations and field data. The depth-averaged turbulent Reynolds stresses of the fluid phase can be considerable where the flow varies rapidly, whilst those of the solid phase are negligible. The present work facilitates a promising depth-averaged two-phase modeling framework for fluvial sediment-laden flows over erodible beds. Yet, inevitable uncertainty of the model arises from the estimations of mass exchange between the flow and the bed as well as bed resistances, which certainly require systematic fundamental investigations of the mechanisms of fluvial sediment-laden flows. Extension to two dimensions is warranted for applications to sediment-laden flows in natural rivers.

Supplementary materials

The Supplementary Materials file consists of three sections concerning (A) derivation of governing equations of the present depth-averaged two-phase model; (B) numerical algorithm for solving the model; (C) case study of bed degradation due to flash floods.

Acknowledgements

This research work is funded by Natural Science Foundation of China under Grants No. 11672212 and 11432015.

References

Ahilan, R. V., Sleath, J., 1987. Sediment transport in oscillatory flow over flat beds. J. Hydraul. Eng.

113(3), 308-322. http://dx.doi.org/10.1061/(ASCE)0733-9429(1987)113:3(308).

Armanini, A., Di Silvio, G., 1988. A one-dimensional model for the transport of a sediment mixture in non-equilibrium conditions. J. Hydraul. Res. 26(3), 275-292. http://dx.doi.org/10.1080/00221688809499212.

Bouchut, F., Fernandez-Nieto, E. D., Mangeney, A., Narbona-Reina, G., 2015. A two-phase shallow debris flow model with energy balance. ESAIM-Math. Model. Numer. Anal. 49(1), 101-140. http://dx.doi.org/10.1051/m2an/2014026.

Bridge, J., Demicco, R., 2008. Earth surface processes, landforms and sediment deposits. Cambridge University Press, Cambridge, UK.

Cao, Z., Hu, P., Hu, K., Pender, G., Liu, Q., 2015a. Modeling roll waves with shallow water equations and turbulent closure. J. Hydraul. Res. 53(2), 161-177. http://dx.doi.org/10.1080/00221686.2014.950350.

Cao, Z., Li, J., Pender, G., and Liu, Q., 2015b. Whole-process modelling of reservoir turbidity currents by a double layer-averaged model. J. Hydraul. Eng. 141(2), 04014069. http://dx.doi.org/10.1061/(ASCE)HY.1943-7900.0000951, 04014069.

Cao, Z., Pender, G., Wallis, S., Carling, P., 2004. Computational dam-break hydraulics over erodible sediment bed. J. Hydraul. Eng. 130(7), 689-703. http://dx.doi.org/10.1061/(ASCE)0733-9429(2004)130:7(689).

Cao, Z., Xia, C., Pender, G., Liu, Q., 2017. Shallow water hydro-sediment-morphodynamic equations for fluvial processes. J. Hydraul. Eng. 143(5), 02517001 (Forum Article). http://dx.doi.org/10.1061/(ASCE)HY.1943-7900.0001281.

Cao Z, Yue Z, Pender G., 2011. Landslide dam failure and flood hydraulics. Part I: experimental investigation. Nat. Hazards, 59(2), 1003-1019. http://dx.doi.org/10.1007/s11069-011-9814-8.

Chauchat, J., Guillou, S., 2008. On turbulence closures for two-phase sediment-laden flow models. J. Geophys. Res. 113, C11017. http://dx.doi.org/10.1029/2007JC004708.

Chien, N., Wan, Z., 1999. Mechanics of sediment transport. ASCE Press, New York.

Chiodi, F., Claudin, P., Andreotti, B., 2014. A two-phase flow model of sediment transport: transition from bedload to suspended load. J. Fluid Mech. 755, 561-581. http://dx.doi.org/10.1017/jfm.2014.422.

Cui, Y. T., Paola, C., Parker, G., 1996. Numerical simulation of aggradation and downstream fining. J. Hydraul. Res. 34(2), 185-204. http://dx.doi.org/10.1080/00221689609498496.

Desmond, K. W., Weeks, E. R., 2014. Influence of particle size distribution on random close packing of spheres. Phys. Rev. E 90(2), 022204. https://doi.org/10.1103/PhysRevE.90.022204.

Deutsch, E, Simonin, O., 1991. Large eddy simulation applied to the motion of particles in stationary homogeneous fluid turbulence. Proc. of ASME-FED. 110, 35-42.

Di Cristo, C., Greco, M., Iervolino, M., Leopardi, A., Vacca, A., 2016. Two dimensional two-phase depth-integrated model for transients over mobile bed. J. Hydraul. Eng. 142(2), 04015043. http://dx.doi.org/10.1061/(ASCE)HY.1943-7900.0001024, 04015043.

Drake, T. G., Shreve, R. L., Dietrich, W. E., Whiting, P. J., Leopold, L. B., 1988. Bedload transport of fine gravel observed by motion-picture photography. J. Fluid Mech. 192, 193-217. https://dx.doi.org/10.1017/S0022112088001831.

Drew, D. A., 1983. Mathematical modelling of two-phase flow. Ann. Rev. Fluid Mech. 15, 261-291. https://dx.doi.org/10.1146/annurev.fl.15.010183.001401

Elghobashi, S., Abou-Arab, T. W., 1983. A two-equation turbulence model for two-phase flows. Phys. Fluids 26, 931-938. https://dx.doi.org/10.1063/1.864243.

Enwald, H., Peirano, E., Almstedt, A. E., 1996. Eulerian two-phase flow theory applied to fluidization. Int. J. Multiphas. Flow 22, 21-66. https://dx.doi.org/10.1016/S0301-9322(96)90004-X.

Fang, H., Wang, G., 2000. Three-dimensional mathematical model of suspended sediment transport. J. Hydraul. Eng. 126(8), 578-592. http://dx.doi.org/10.1061/(ASCE)0733-9429(2000)126:8(578).

Ferguson, R. I., Wathen, S. J., 1998. Tracer-pebble movement along a concave river profile: Virtual velocity in relation to grain size and shear stress. Water Resour. Res. 34(8), 2031-2038. http://dx.doi.org/10.1029/98WR01283.

Frey, P., Church, M., 2009. How river beds move. Science 325(5947), 1509-1510. http://dx.doi.org/10.1126/science.1178516.

Gidaspow, D., 1994. Multiphase Flow and Fluidization: Continuum and Kinetic Theory Descriptions. Academic Press, San Diego, USA.

Gray, J. M. N. T., Chugunov, V. A., 2006. Particle-size segregation and diffusive remixing in shallow granular avalanches. J. Fluid Mech. 569, 365-398. http://dx.doi.org/10.1017/S0022112006002977.

Greco, M., Iervolino, M., Leopardi, A., Vacca, A., 2012. A two-phase model for fast geomorphic shallow flows. Int. J. Sediment Res. 27(4), 409-425. http://dx.doi.org/10.1016/S1001-6279(13)60001-3.

Greimann, B. P., 2003. Two-phase flow analysis of sediment velocity. In: Gyr, A., Kinzelbach, W. (eds), Sedimentation and Sediment Transport. Springer, Netherlands, pp. 83-86,

Greimann, B. P., Holly Jr, F. M., 2001. Two-phase flow analysis of concentration profiles. J. Hydraul. Eng. 127(9), 753-762. http://dx.doi.org/10.1061/(ASCE)0733-9429(2001)127:9(753).

Greimann, B., Lai, Y., Huang, J. C., 2008. Two-dimensional total sediment load model equations. J. Hydraul. Eng. 134(8), 1142–1146. http://dx.doi.org/10.1080/00221686.1999.9628264.

Greimann, B. P., Muste, M., Holly Jr, F. M., 1999. Two-phase formulation of suspended sediment transport. J. Hydraul. Res. 37(4), 479-500. http://dx.doi.org/10.1080/00221686.1999.9628264.

Guan, M., Wright, N. G., Sleigh, P. A., Ahilan, S., Lamb, R., 2016. Physical complexity to model morphological changes at a natural channel bend. Water Resour. Res. 52, 6348-6364, http://dx.doi.org/10.1002/2015WR017917.

Guo, Q. C., Jin, Y. C., 1999. Modeling sediment transport using depth-averaged and moment equations. J. Hydraul. Eng. 125(12), 1262-1269. http://dx.doi.org/10.1061/(ASCE)0733-9429(1999)125:12(1262).

Haschenburger, J. K., Church, M., 1998. Bed material transport estimated from the virtual velocity of sediment. Earth Surf. Proc. Land. 23(9), 791-808. http://dx.doi.org/10.1002/(SICI)1096-9837(199809)23:9<791::AID-ESP888>3.0.CO;2-X.

Hill, K. M., Tan, D. S., 2014. Segregation in dense sheared flows: gravity, temperature gradients, and stress partitioning. J. Fluid Mech. 756, 54-88. http://dx.doi.org/10.1017/jfm.2014.271.

Hirano, M., 1971. River bed degradation with armouring. Trans. Japanese Soc. Civ. Eng. 195, 55-65.

Hoey, T. B., Ferguson, R., 1994. Numerical simulation of downstream fining by selective transport in gravel bed rivers: Model development and illustration. Water Resour. Res. 30(7), 2251-2260. http://dx.doi.org/10.1029/94WR00556.

Hsu, T. J., Jenkins, J. T., Liu, P. L. F., 2003. On two-phase sediment transport: Dilute flow. J. Geophys. Res. 108(C3), 3057. http://dx.doi.org/10.1029/2001JC001276.

Hu, P., Cao, Z., Pender, G., Liu, H., 2014. Numerical modelling of riverbed grain size stratigraphic evolution. Int. J. Sediment Res. 29(3), 329-343. http://dx.doi.org/10.1016/S1001-6279(14)60048-2.

Huang, W., Cao, Z., Yue, Z., Pender, G., Liu, Q., Carling, P., 2015. Coupled flood and sediment transport modeling with adaptive mesh refinement. Sci. China Technol. Sc. 58(8), 1425-1438. http://dx.doi.org/10.1007/s11431-015-5880-6.

Iverson, R. M., Ouyang, C., 2015. Entrainment of bed material by earth surface mass flows: Review and reformulation of depth-integrated theory. Rev. Geophys. 53(1), 27-58. http://dx.doi.org/10.1002/2013RG000447.

Jenkins, J. T., Richman, M. W., 1985. Grad's 13 moment system for a dense gas of inelastic spheres. Arch. Ratio. Mech. Anal. 87, 355-377. http://dx.doi.org/10.1007/978-3-642-61634-1_31.

Launder, B. E., Spalding, D. B., 1974. The numerical computation of turbulent flows. Comput. Meth.

Appl. Mech. Eng. 3, 269-289. http://dx.doi.org/10.1007/978-3-642-61634-1_31.

Li, J., Cao, Z., Pender, G., Liu, Q., 2013. A double layer-averaged model for dam-break flows over mobile bed. J. Hydraul. Res. 51(5), 518-534. http://dx.doi.org/10.1080/00221686.2013.812047.

Lenzi, M. A., 2004. Displacement and transport of marked pebbles, cobbles and boulders during floods in a steep mountain stream. Hydrol. Process 18(10), 1899-1914. http://dx.doi.org/10.1002/hyp.1456.

Longo, S., 2005. Two-phase flow modeling of sediment motion in sheet-flows above plane beds. J. Hydraul. Eng. 131(5), 366-379.

Marsooli, R., Wu, W., 2015. Three-dimensional numerical modeling of dam-break flows with sediment transport over movable beds. J. Hydraul. Eng. 141(1), 04014066. http://dx.doi.org/10.1061/(ASCE)HY. 1943-7900.0000947, 04014066.

Muste, M., Yu, K., Fujita, I., Ettema, R., 2005. Two-phase versus mixed-flow perspective on suspended sediment transport in turbulent channel flows. Water Resour. Res. 41, W10402. http://dx.doi.org/10.1029/2004WR003595.

Pai, S. I., 1977. Two-phase flows. Springer-Verlag, Berlin, Germany.

Paola, C., Parker, G., Seal, R., Sinha, S. K., Southard, J. B., Wilcock, P. R., 1992. Downstream fining by selective deposition in a laboratory flume. Science 258, 1757-1757.

Parker, G., 1991a. Selective Sorting and Abrasion of River Gravel. I: Theory. J. Hydraul. Eng. 117, 131-147. http://dx.doi.org/10.1061/(ASCE)0733-9429(1991)117:2(131).

Parker, G., 1991b. Selective Sorting and Abrasion of River Gravel. II: Applications. J. Hydraul. Eng. 117, 150-171. http://dx.doi.org/10.1061/(ASCE)0733-9429(1991)117:2(150).

Pelanti, M., Bouchut, F., Mangeney, A., 2008. A Roe-Type scheme for two-phase shallow granular flows over variable topography. ESAIM-Math. Model. Numer. Anal. 42, 851-885. http://dx.doi.org/10.1051/m2an:2008029.

Pitman, E. B., Le, L., 2005. A two-fluid model for avalanche and debris flows. Proc. R. Soc. A-Math. Phys. Eng. Sci. 363, 1573-1602. http://dx.doi.org/10.1098/rsta.2005.1596.

Pudasaini, S. P., 2012. A general two-phase debris flow model. J. Geophys. Res. 117, F03010. http://dx.doi.org/10.1029/2011JF002186.

Qian, H., Cao, Z., Pender, G., Liu, H., Hu, P., 2015. Well-balanced numerical modeling of non-uniform sediment transport in alluvial rivers. Int. J. Sediment Res. 30(2), 117-130. http://dx.doi.org/10.1016/j.ijsrc.2015.03.002.

Rastogi, A. K., Rodi, W., 1978. Predictions of heat and mass transfer in open channels. J. Hydraul.

Div. 104(3), 397-420. http://dx.doi.org/10.1061/9780784403891.006.

Reid, I., Laronne, J. B., Powell, D. M., 1995. The Nahal Yatir bedload database: Sediment dynamics in a gravel-bed ephemeral stream. Earth Surf. Proc. Land 20(9), 845-857. http://dx.doi.org/10.1002/esp.3290200910.

Savage, S. B., Hutter, K., 1989. The motion of a finite mass of granular material down a rough incline. J. Fluid Mech. 199, 177-215. http://dx.doi.org/10.1017/S0022112089000340.

Seal, R., Paola, C., Parker, G., Southard, J. B., Wilcock, P. R., 1997. Experiments on downstream fining of gravel: I. Narrow-channel runs. J. Hydraul. Eng. 123(10), 874-884. http://dx.doi.org/10.1061/(ASCE)0733-9429(1997)123:10(874).

Simonin, O., 1991. Prediction of the dispersed phase turbulence in particle-laden jets. The 4th International Symposium on Gas-Solid Flows, ASME FED, Portland.

Simonin O, Viollet P. L., 1990. Numerical study on phase dispersion mechanisms in turbulent bubbly flows. In: Sommerfeld, M., Wennerberg, D. (Eds.), Fifth Workshop on Two-Phase Flow Predictions. Forsch, Senckenberg, pp. 156-166.

Toro-Escobar, C. M., Paola, C., Parker, G., 1996. Transfer function for the deposition of poorly sorted gravel in response to streambed aggradation. J. Hydraul. Res. 34, 35-53. http://dx.doi.org/10.1080/00221689609498763.

Torquato, S., 1995. Nearest-neighbor statistics for packings of hard spheres and disks. Phys. Rev. E 51(4), 3170. https://doi.org/10.1103/PhysRevE.51.3170.

Torquato, S., Stillinger, F. H., 2007. Toward the jamming threshold of sphere packings: Tunneled crystals. J. Appl. Phys. 102(9), 093511. http://dx.doi.org/10.1063/1.2802184.

Torquato, S., Stillinger, F. H., 2010. Jammed hard-particle packings: From Kepler to Bernal and beyond. Rev. Mod. Phys. 82(3), 2633. https://doi.org/10.1103/RevModPhys.82.2633.

Uchida, T., Fukuoka, S., 2014. Numerical calculation for bed variation in compound-meandering channel using depth integrated model without assumption of shallow water flow. Adv. Water Resour. 72, 45-56. http://dx.doi.org/10.1016/j.advwatres.2014.05.002.

Van Rijn, L. C., 1986. Mathematical modeling of suspended sediment in nonuniform flows. J. Hydraul. Eng. 112(6), 433-455. http://dx.doi.org/10.1061/(ASCE)0733-9429(1986)112:6(433).

Vasquez, J. A., Millar, R. G., Steffler, P. M., 2011. Vertically-averaged and moment model for meandering river morphology. Can. J. Civil Eng. 38(8), 921-931. http://dx.doi.org/10.1139/l11-063.

Viparelli, E., Sequeiros, O. E., Cantelli, A., Wilcock, P. R., Parker, G., 2010. River morphodynamics with creation/consumption of grain size stratigraphy 2: Numerical model. J. Hydraul. Res. 48(6), 727-741. http://dx.doi.org/10.1080/00221686.2010.526759.

Wilcock, P. R., 1997. Entrainment, displacement and transport of tracer gravels. Earth Surf. Proc. Land. 22(12), 1125-1138. http://dx.doi.org/10.1002/(SICI)1096-9837(199712)22:12<1125.

Wu, W., 2004. Depth-averaged two-dimensional numerical modeling of unsteady flow and nonuniform sediment transport in open channels. J. Hydraul. Eng. 130(10), 1013-1024. http://dx.doi.org/10.1061/(ASCE)0733-9429(2004)130:10(1013).

Wu, W., 2007. Computational river dynamics. Taylor and Francis, London, UK.

Wu, W., Rodi, W., Wenka, T., 2000. 3D numerical modeling of flow and sediment transport in open channels. J. Hydraul. Eng. 1(4), 4-15. http://dx.doi.org/10.1061/(ASCE)0733-9429(2000)126:1(4).

Wu, W., Wang, S. S. Y., 2006. Formulas for sediment porosity and settling velocity. J. Hydraul. Eng. 132(8), 858-862. http://dx.doi.org/10.1061/(ASCE)0733-9429(2006)132:8(858).

Wu, W. M., Altinakar, M., Wang, S. S. Y., 2006. Depth-average analysis of hysteresis between flow and sediment transport under unsteady conditions. Int. J. Sediment Res. 21(2), 101–112.

Wu, W. M., Wang, S. S. Y., 2008. One-dimensional explicit finite-volume model for sediment transport. J. Hydraul. Res. 46(1), 87-98. http://dx.doi.org/10.1080/00221686.2008.9521846.

Xia, C., Jin, Y. C., 2006. Multilayer averaged and moment equations for one-dimensional open-channel flows. J. Hydraul. Eng. 132(8), 839-849. http://dx.doi.org/10.1061/(ASCE)0733-9429(2006)132:8(839).

Yeh, K. C., Kennedy, J. F., 1993. Moment model of nonuniform channel-bend flow. II: Erodible beds. J. Hydraul. Eng. 119(7), 796-815. https://doi.org/10.1061/(ASCE)0733-9429(1993)119:7(796).

Zech, Y., Soares-Frazao, S., Van Emelen, S., 2015. Modelling of fast hydraulic transients: Issues, challenges, perspectives. La Houille Blanche 5, 5-15. http://dx.doi.org/10.1051/lhb/20150049.

Zhang, R. J., Xie, J. H., 1993. Sedimentation research in China-systematic selections. China Water and Power Press, Beijing, P. R. China.

List of figure captions

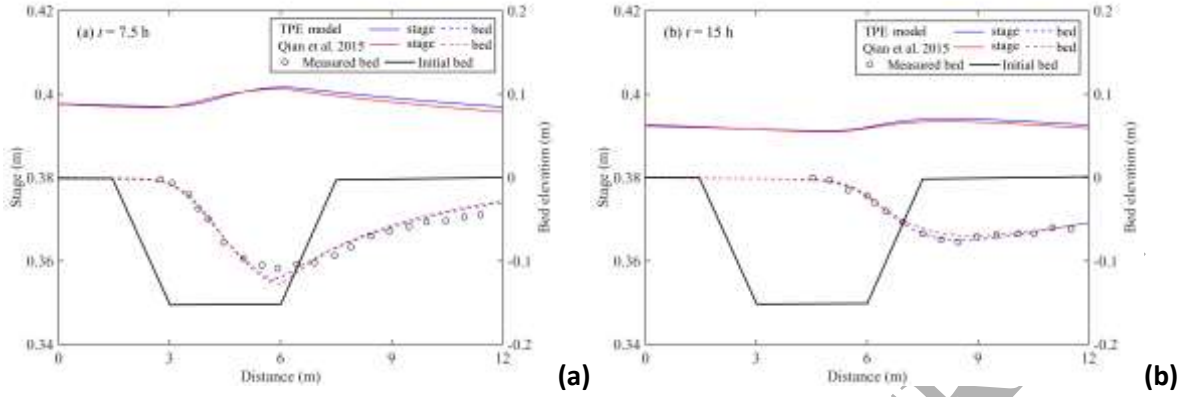

Fig.1. Computed stage and bed profiles at (a) $t = 7.5$ h; (b) $t = 15$ h from the TPE model and Qian et al. (2015) along with the measured bed profiles.

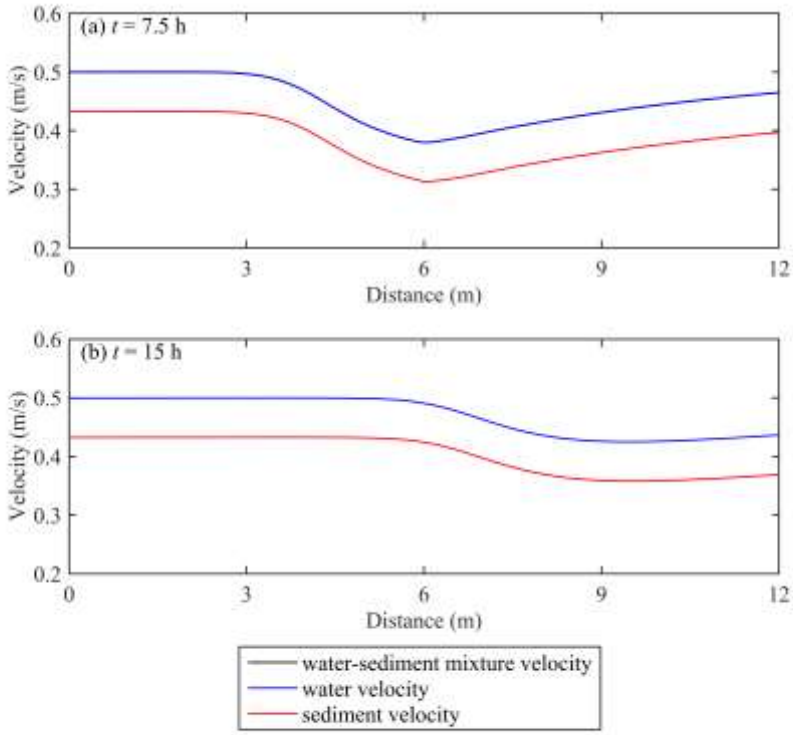

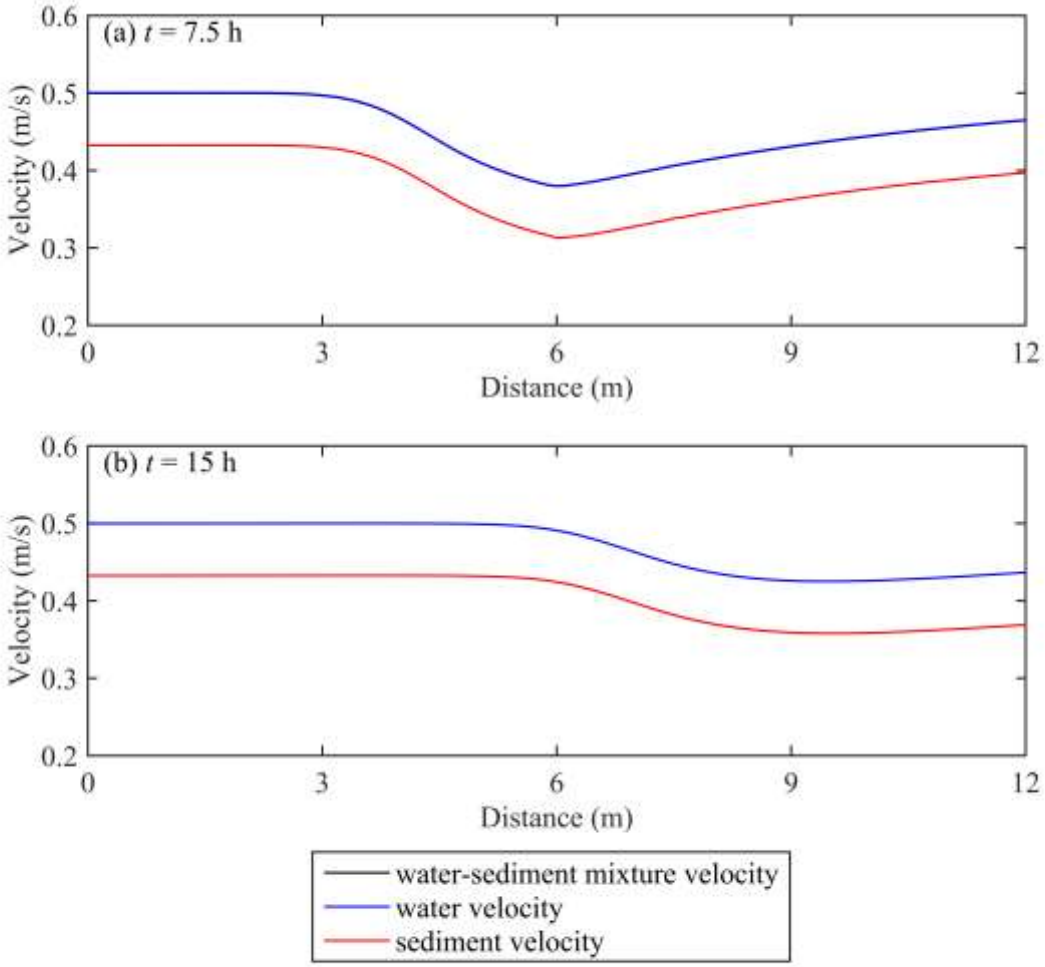

Fig. 2. Computed depth-averaged longitudinal velocity profiles of the water-sediment mixture, fluid and sediment phases from the TPE model. The velocities of the water-sediment mixture (black line) and the fluid phase (blue line) are indistinguishable.

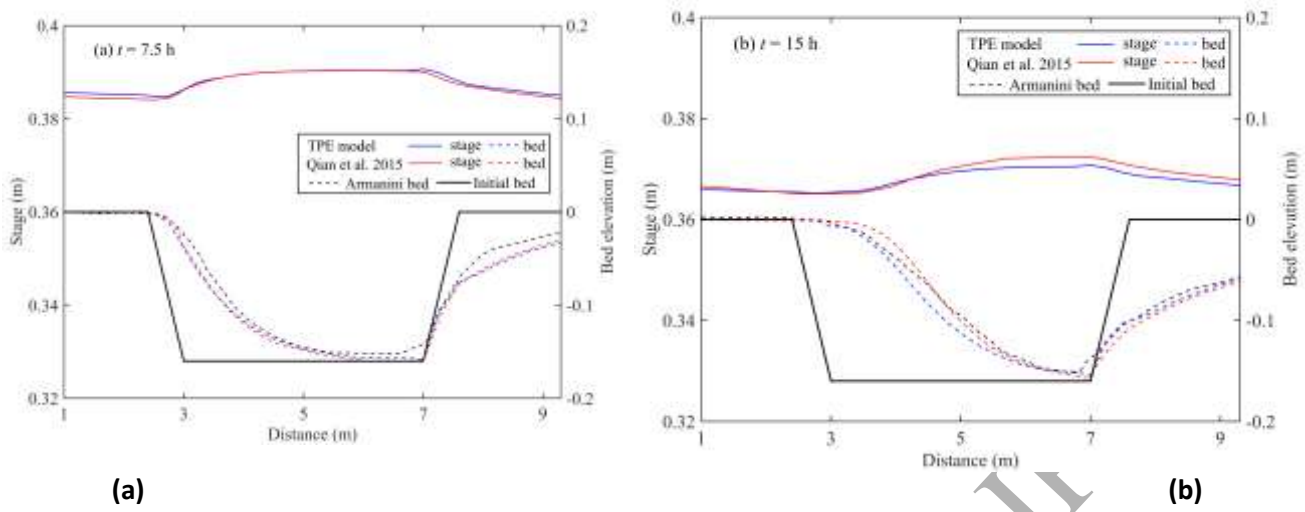

(a) **(b)**

Fig. 3. Computed stage and bed profiles at (a) $t = 7.5$ h; (b) $t = 15$ h from the TPE model and Qian et al. (2015) along with the bed profiles from Armanini and Di Silvio (1988).

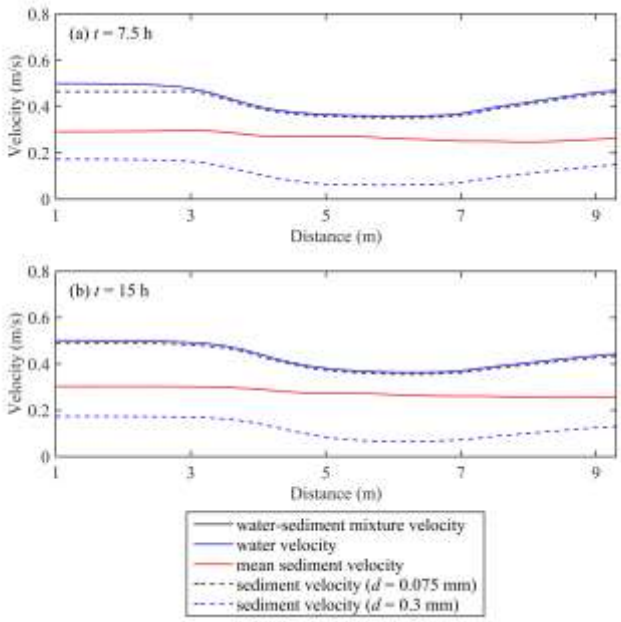

Fig. 4. Computed depth-averaged longitudinal velocity profiles of the water-sediment mixture, fluid, and the size-specific sediment phases along with the profiles of the depth-averaged mean sediment velocity from the TPE model. The velocities of the water-sediment mixture (black line) and the fluid phase (blue line) are indistinguishable.

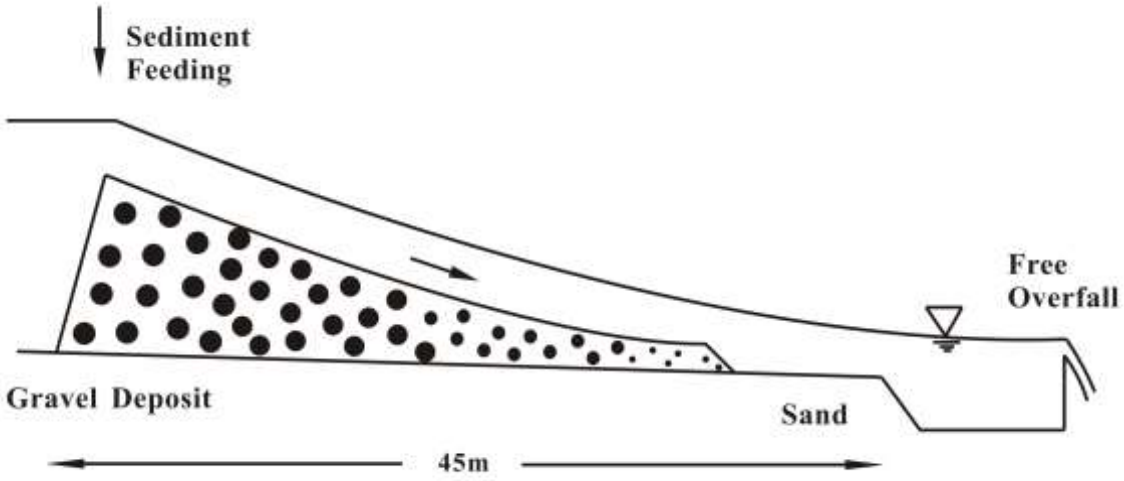

Fig. 5. Sketch of the aggradation experiment [adapted from Seal et al. (1997)].

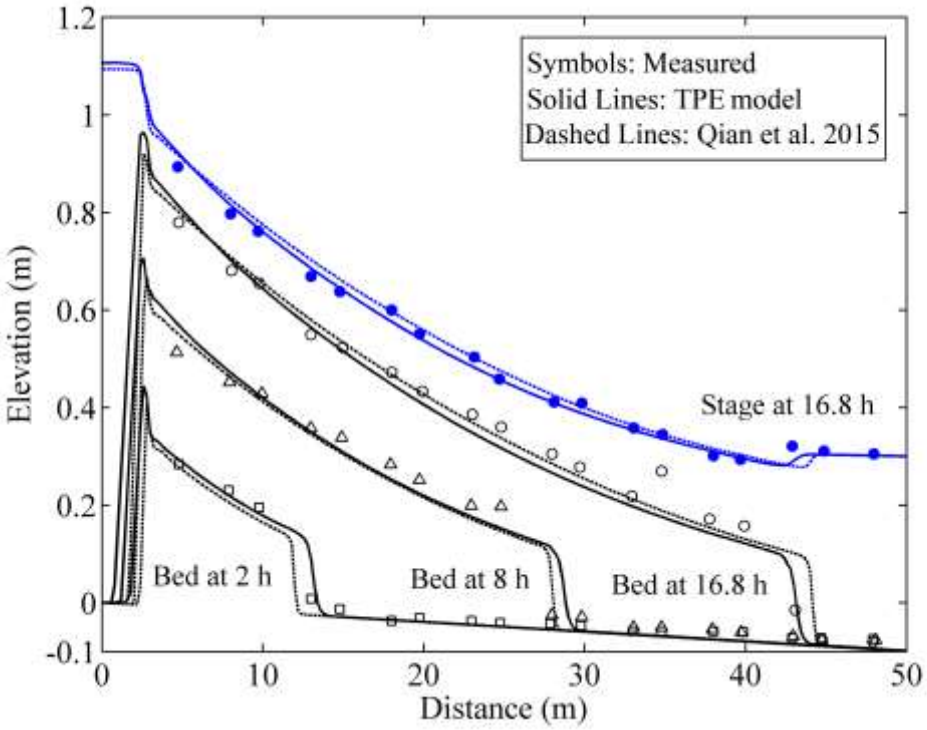

Fig. 6. Computed stage and bed profiles compared to measured data.

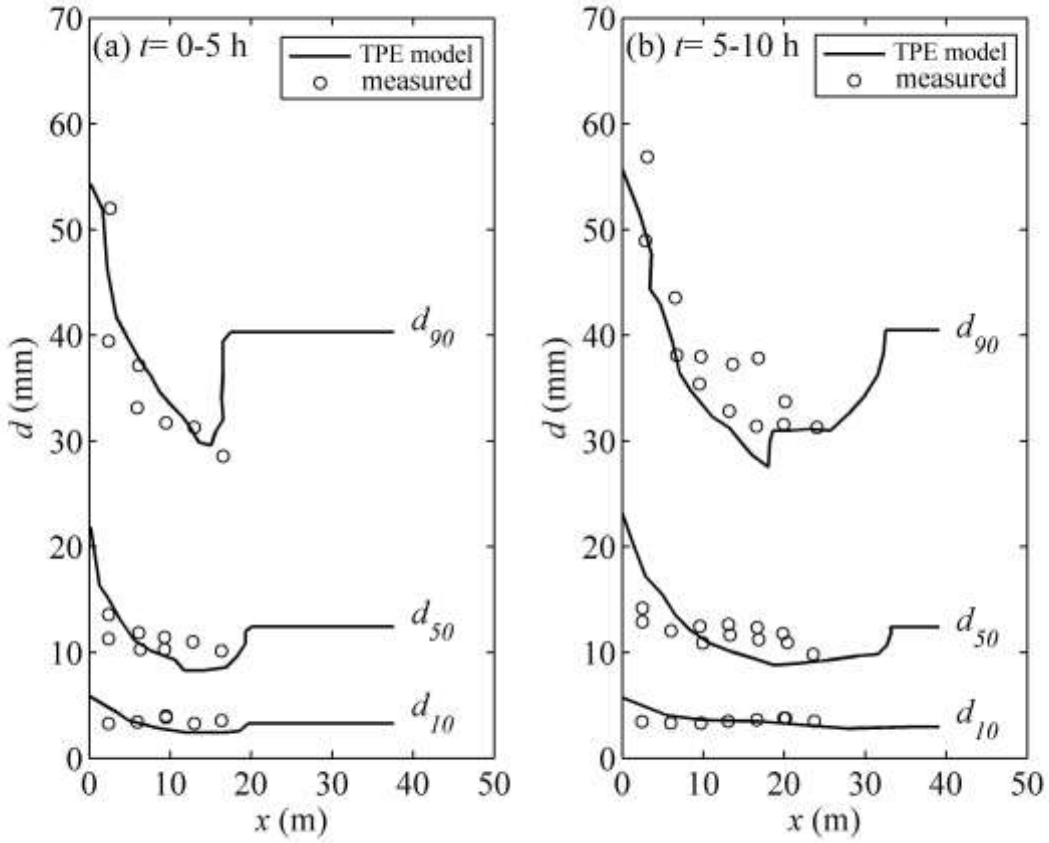

Fig. 7. Computed characteristic sizes of the deposition from TPE model in comparison with measured data.

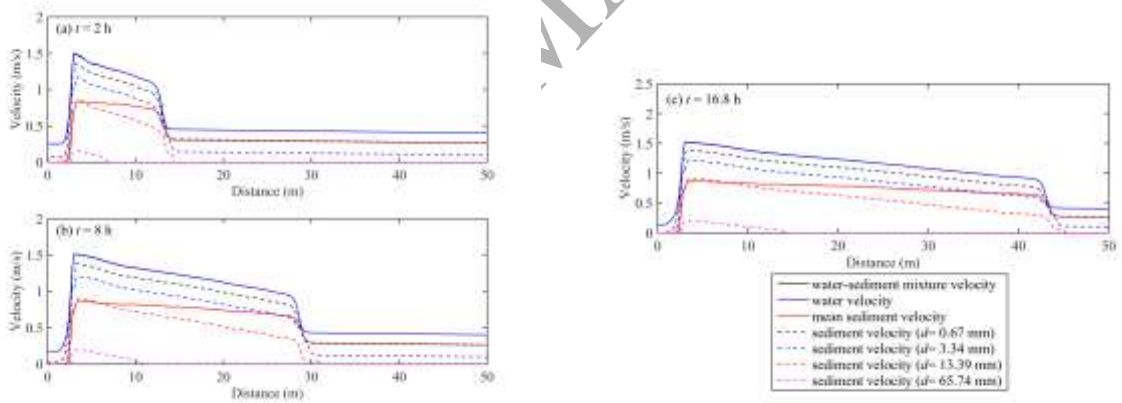

(a) **(b)**

Fig. 8. Computed depth-averaged longitudinal velocity profiles of the water-sediment mixture, fluid and selected size-specific sediment phases along with the profiles of the depth-averaged mean sediment velocity from the TPE model. Indistinguishable velocity discrepancy can be spotted between the water-sediment mixture (black line) and the fluid phase (blue line).

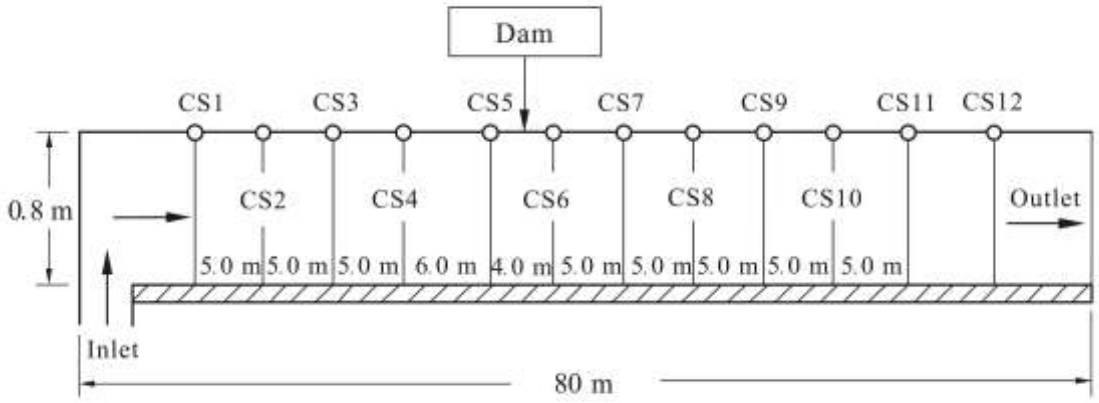

Fig. 9. Experimental set-up for landslide dam failure [adapted from Li et al. (2013)].

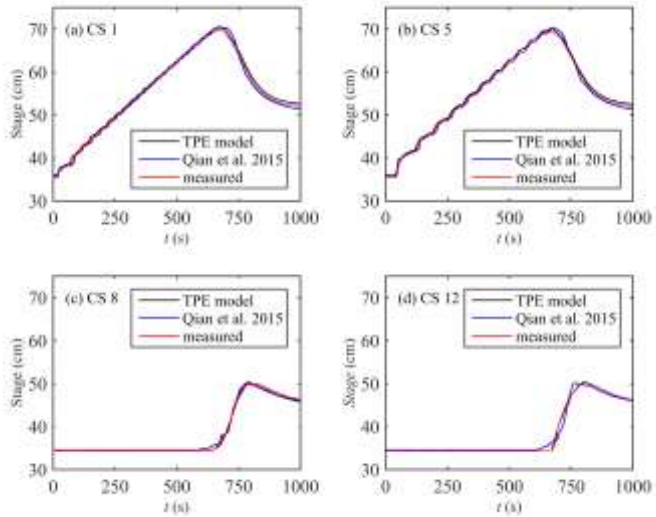

Fig. 10. Computed stage hydrographs from TPE model and Qian et al. (2015) against measured data.

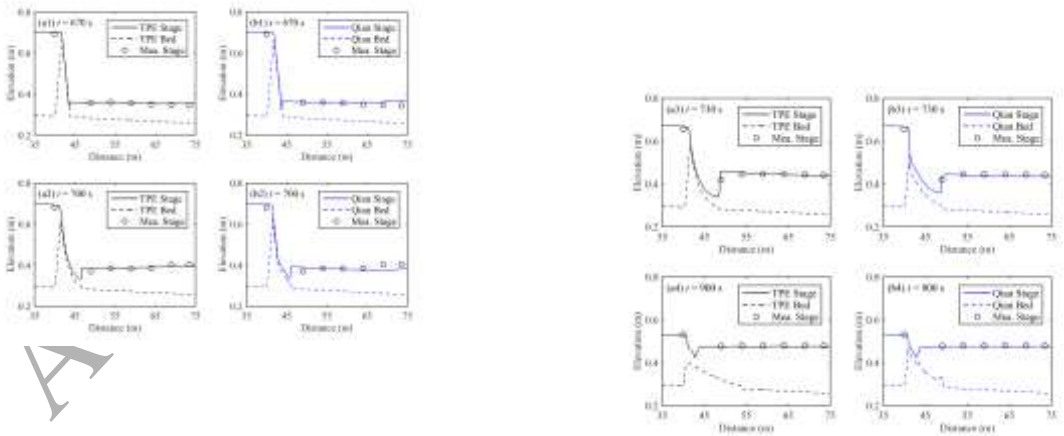

(a) **(b)**

Fig. 11. Computed stage and bed profiles from TPE model (a1-a4) and Qian et al. (2015) (b1-b4) along with the measured data for stage.

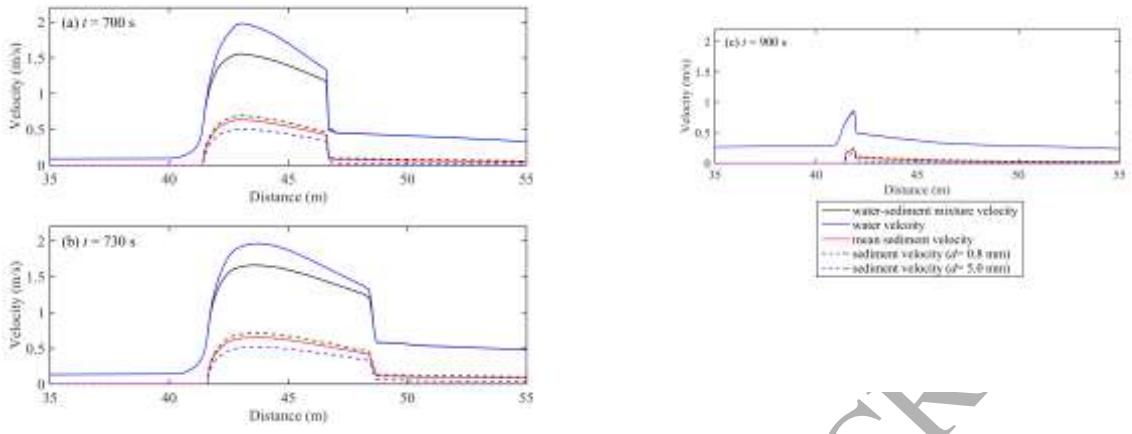

(a) **(b)**

Fig. 12. Computed depth-averaged longitudinal velocity profiles of the water-sediment mixture, fluid and sediment phases along with the profiles of the depth-averaged mean sediment velocity. Appreciable velocity difference between the water-sediment mixture (black line) and fluid phase (blue line) can be spotted in (b) and (c).

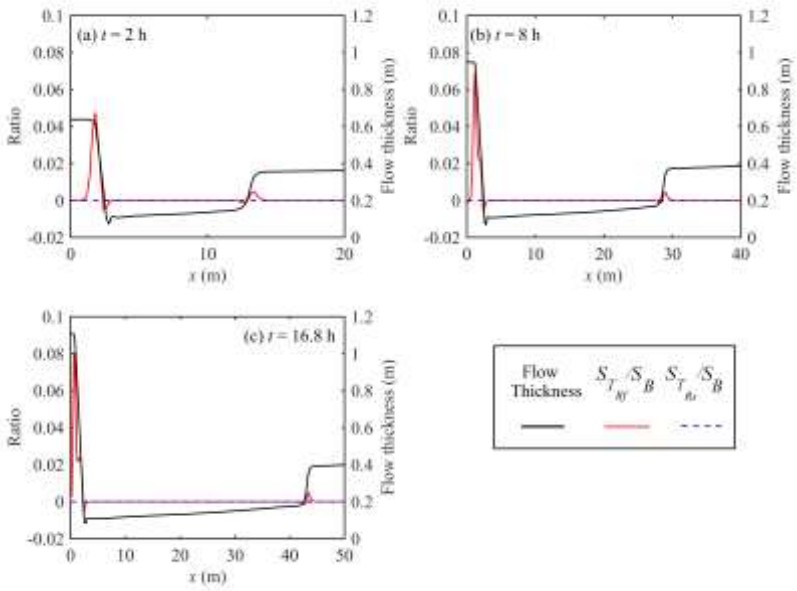

Fig. 13. Computed depth-averaged turbulent Reynolds stresses compared with the frictional term (Case 3).

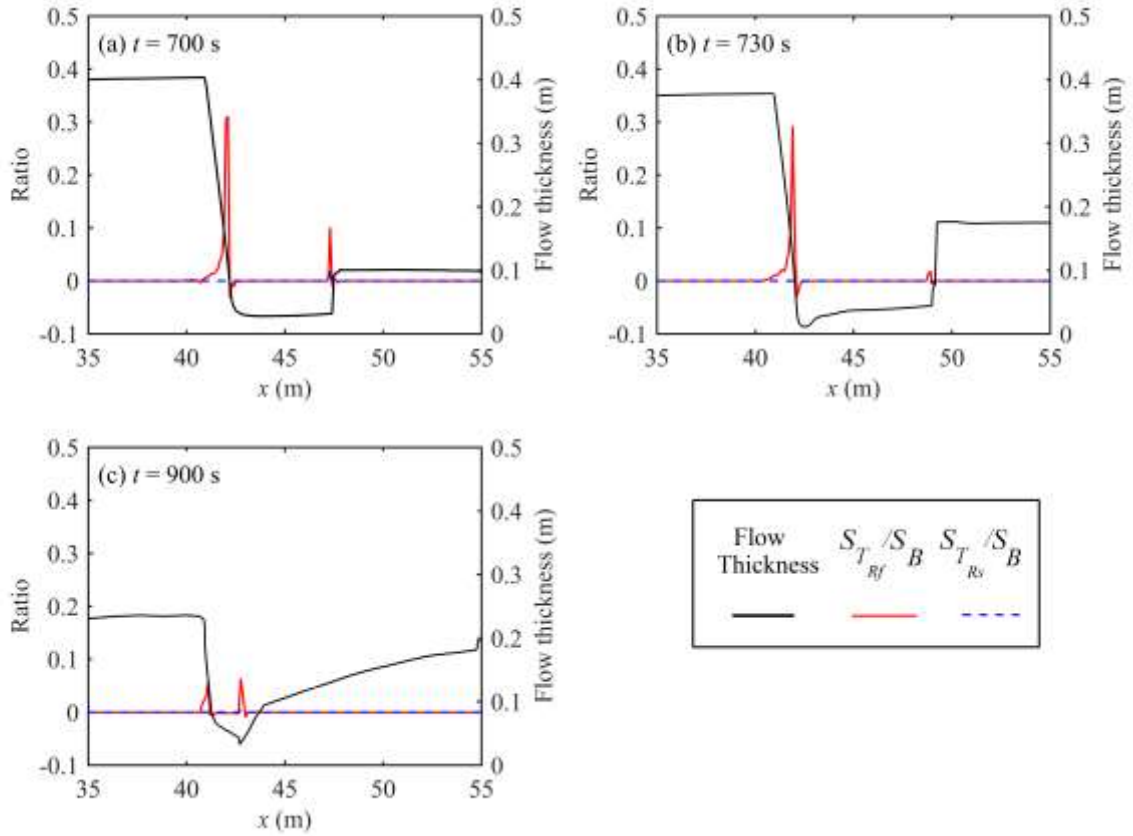

Fig. 14. Computed depth-averaged turbulent Reynolds stresses compared with the frictional term (Case 4).